A Small-Angle Neutron and X-ray Contrast Variation Scattering Study of the Structure of Block Copolymer Micelles: Corona Shape and Excluded Volume Interactions

Jan Skov Pedersen,*,† Carsten Svaneborg,‡ Kristoffer Almdal,‡ Ian W. Hamley,§ and Ron N. Young||

Department of Chemistry, University of Aarhus, DK-8000 Aarhus C, Denmark, Danish Polymer Center, Risø National Laboratory, DK-4000 Roskilde, Denmark, School of Chemistry, University of Leeds, Leeds LS2 9JT, W. Yorkshire, England, and Department of Chemistry, University of Sheffield, Sheffield S3 7HF, S. Yorkshire, England

Received March 28, 2002; Revised Manuscript Received October 7, 2002

ABSTRACT: Small-angle neutron and X-ray scattering data have been obtained for micelles of *d*-polystyrene−polyisoprene (*d*-PS−PI) of relatively high molecular weight in *n*-decane. Contrast variation was performed using mixtures of hydrogenated and deuterated decane. Three samples were investigated with *d*-polystyrene and polyisoprene molar masses of, respectively, 12 000 and 48 000, 40 000 and 40 000, and 40 000 and 80 000. For the two latter samples, the concentration of the polymer was also varied. The data obtained at relatively high resolution were analyzed together with small-angle X-ray scattering data using scattering functions recently derived from Monte Carlo simulations for a model with a spherical core and a corona of semiflexible chains interacting with a hard-core potential. The scattering from the model can be generated by assuming an analytical form of the radial distribution of the corona and an effective single chain form factor of the random-phase approximation type. In the analysis of the experimental scattering data intermicellar interactions were modeled by an effective hard-sphere model. The analysis of the experimental data provides information on shape, aggregation number, polydispersity, core size, core solvation, corona shape/size, and the interactions between the chains in the corona, which are significant for these micelles. The shape of the corona profile depends on the surface coverage of the micelles as well as the curvature of the core−corona interface. For high curvatures the profile is in agreement with a power-law behavior as predicted by scaling theory. For low curvatures the profile is more compact. The profiles and scattering curves are very well reproduced by Monte Carlo simulations based on the parameters for the structures determined in the analysis of the experimental scattering data. The study shows that two parameters are decisive for the profile shape and internal correlations, namely the reduced surface coverage and the curvature.

1. Introduction

Studies of stability and rheology of colloidal suspensions are scientific disciplines of great technological importance. Colloids consist of nanosize particles, and these are often sterically stabilized by layers of grafted chains or polymers. These layers govern the form of the interparticle potential, which results in the actual stability and rheological properties of the suspensions. It is therefore highly technological relevant to study the structure and interactions of systems consisting of particles with grafted polymers. One such system is block copolymers in a selective solvent, which is studied in the present work.

Block copolymers are constituted of two chemically distinct polymer blocks covalently bonded together. When dissolved in a solvent which is a selective solvent for one block, micelles are formed with a core of the nonsoluble parts and a diffuse corona of the soluble chains.[1] During the last couple of decades, there has been intensive work theoretically and experimentally on the structure of such micelles. The theoretical work has employed different approaches, for example, self-consistent field calculations,[2,3] Monte Carlo simulations,[4−7] and scaling theory.[8,9] The aim of the studies has been to determined the radial profile of the corona as a function of chain length and surface coverage. The most suitable method for experimentally determining the radial profile is the small-angle scattering technique.[10] A particular powerful approach is contrast-variation small-angle neutron scattering (SANS). This technique can be used if the two blocks of the polymer have distinctly different scattering length densities, as they have, for example, when one of the blocks is perdeuterated. The contrast is varied by varying the scattering density of the solvent by mixing protonated and deuterated solvents.[3,11−17] In this way the two parts of the micelle, the core and the corona, can be highlighted by selectively contrast matching one of the parts.

In most contrast variation studies the scattering data have been analyzed by models which assume centrosymmetry of the micelles. Similar models have been used in other recent studies of block copolymer micelles;[18−24] however, for most contrasts these models do not describe the observed scattering at high scattering vectors. Richter et al.[12] included an empirical term for describing the "blob" scattering originating from the dissolved chains in the corona which surrounds the core of the micelles. This scattering contribution is included explicitly in the models of the type described by Pedersen and Gerstenberg.[17,25−27] In these models the chains are assumed to obey Gaussian statistics and to be noninteracting and this allows the form factor to be

* Author for correspondence.
† University of Aarhus.
‡ Risø National Laboratory.
§ University of Leeds.
|| University of Sheffield.

10.1021/ma0204913 CCC: $25.00 © 2003 American Chemical Society
Published on Web 12/17/2002

calculated analytically. Core expulsion of the corona chains is mimicked by moving the center of mass of the chains away from the surface. This model has successfully been applied in the analysis of scattering data from block copolymer micelles.[17,25,27,28,30,31] As the chains are assumed to be noninteracting, the profile of the corona is always "mushroom"-like with the highest density at a distance of about R_g away from the core surface, where R_g is the radius of gyration of the chains.[17,27,28]

Monte Carlo simulations on semiflexible polymer models with hard-core excluded volume effects have led to significant advances in the analysis of scattering data from linear homopolymers at dilute and semidilute concentration.[32−34] Encouraged by this, a simulation study of a micellar model with semiflexible hard-core corona chains was recently initiated.[5] In the model used in this study, all interactions between chains and between chains and core were taken into account and described by hard-sphere potentials. In the study, the various contributions to the scattering function were sampled and combined to give the form factor of the micelle for a broad variation of parameters, like chain length, surface coverage and effective curvature of the core−corona interface. It was shown,[6] that the effects of interactions on the single chain behavior can be described by a random-phase approximation (RPA) expression. Additional effects were present in the terms related to the radial profile of the corona. In a subsequent publication,[7] it was demonstrated that the radial profile could be well approximated by simple analytical expressions. From a fit of these expressions to the sampled scattering functions and comparison to the directly sampled radial profiles, it was concluded that the model could be used for obtaining the radial profile as well as information on the interactions between the polymers in the corona from experimental data.

Relatively few detailed studies have previously been made of polymer corona profile shapes by small-angle scattering. Förster et al.[35] analyzed their data from micelles of polystyrene-*b*-poly(4-vinylpyridine) using a power-law profile and found exponents in the range from −1.35 to −1.04. Won et al.[36] investigated micelles of poly(ethylene oxide)-*b*-polybutadiene micelles in water and used a Fermi-Dirac-type function for the profile. They found concave profiles, which are similar in shape to power-law profiles. Willner et al.[37] studied micelles of poly(ethylene−propylene)-*b*-poly(ethylene oxide) (PEP−PEO) in water and used a power-law profile with a Fermi−Dirac-type cutoff function for analyzing the data. They found a crossover from a constant density to a power-law behavior with an exponent of −1.3 on increasing length of the PEO chains in the corona. It is only in this latter work that an empirical term for describing the "blob" scattering originating from the dissolved chains in the corona is included. The other models are purely centrosymmetric.

In the present paper we present a SANS contrast variation study of the micellar structure of PS−PI micelles in decane which is a strongly selective solvent for PI. Micelles of block copolymers with a deuterated PS block (*d*-PS−PI) were investigated in detail in mixtures of deuterated and protonated *n*-decane. The SANS measurements were supplemented by small-angle X-ray scattering (SAXS) measurements, which were also used for checking for isotope effects. Polymers with three different relatively high molecular weights were studied. By simultaneous fitting of scattering data for the four different contrasts measured for each sample, the structures of the micelles were determined.

As already mentioned, the analysis described in the present paper is based on recent Monte Carlo simulations. The model is thus on a much more firm ground than previously used models and we can therefore expect to obtain more information, which is more reliable, than in previous studies. We note that the expressions for the scattering intensity go beyond centrosymmetric models and include a self-consistent description of the "blob" scattering originating from the correlations within the corona, i.e., from chain connectivity, chain−chain, and chain−core interactions. In the analysis, we use a series of different methods for parametrizing the radial profile of the corona. This is done with the purpose of estimating the systematic errors on the profiles imposed by the used parametrization. We have also used power-law profiles in order to check the agreement with the predictions of scaling theory.[9]

2. Experimental Section

Samples: Polymers and Solvents. The two *d*-PS−PI block copolymers with nominal molecular weights of 40 000−40 000 and 40 000−80 000, respectively, were synthesized by anionic polymerization in the Department of Chemistry, University of Sheffield. The two polymers are denoted 40−40 and 40−80, respectively, in the rest of the paper. The diblock copolymers were synthesized under rigorous high vacuum conditions in all-glass reactors.[38] Isoprene was purified by treatment with solvent-free dibutylmagnesium for 24 h followed by distillation from solvent-free *n*-butyllithium after contact for 30 min at −15 °C. Styrene-d_8 with 98% deuteration was similarly distilled from solvent-free dibutylmagnesium after standing for 24 h. Tetrahydrofuran (THF) was distilled from sodium/potassiun alloy to which a little benzophenone had been added; the purple dinegative ion of the latter served to confirm perfect dryness. Cyclohexane was distilled from an orange solution of oligomeric styryllithium. *sec*-Butyllithium (*sec*-BuLi) was distilled in a short path length apparatus under high vacuum, and a solution was prepared in cyclohexane; the concentration was determined by hydrolysis and titration of an aliquot. The polyisoprene block was polymerized in cyclohexane using *sec*-BuLi as initiator. After 24 h a sample was withdrawn for analysis. The styrene monomer was then introduced together with a little THF; the latter ensured that the initiation of the formation of the second block was virtually instantaneous. Polymerization was allowed to proceed for 12 h whereupon the active chain ends were terminated by the introduction of degassed methanol. The molecular weights and polydispersities were determined by size exclusion chromatography with a triple detector system and NMR measurements. This gave for 40−40 a molecular weight of *d*-PS of $M_w(d\text{-PS}) = 45 \times 10^3$ g mol^{-1}, and of the PI of $M_w(\text{PI}) = 41 \times 10^3$ g mol^{-1}, and $M_w/M_n \approx 1.03$. For the 40−80, $M_w(d\text{-PS}) = 51 \times 10^3$ g mol^{-1}, $M_w(\text{PI}) = 80 \times 10^3$ g mol^{-1}, and $M_w/M_n < 1.04$. In addition a deuterated polystyrene-d_8−polyisoprene diblock, custom synthesized by Polymer Source Inc. (Dorval, Canada), was used. The molecular weights and polydispersity determined by the manufacturer using size exclusion chromatography were $M_w(d\text{-PS}) = 11.5 \times 10^3$ g mol^{-1}, $M_w(\text{PI}) = 48.5 \times 10^3$ g mol^{-1}, and $M_w/M_n < 1.15$. This polymer is denoted 12−48 in the following.

The neutron scattering length density of *d*-PS, $\rho_{d-\text{PS}} = 6.42 \times 10^{10}$ cm^{-2} was calculated for a density of 1.12 g/cm^3 and a deuteration degree of 98%. For the protonated PI $\rho_{\text{PI}} = -0.274 \times 10^{10}$ cm^{-2} for a density of 0.93 g/cm^3. The scattering length densities for SAXS are proportional to the electron densities. These are for PS, PI, and decane, respectively, 0.337, 0.313, and 0.254 e/Å^3. This gives the excess electron densities 0.083 and 0.059 e/Å^3 for PS and PI, respectively.

Protonated *n*-decane was obtained from Sigma and the perdeuterated *n*-decane was obtained from Chemotrade, Leipzig,

Germany. The density of protonated *n*-decane is 0.730 g/cm^3 and the neutron scattering length density is $\rho_{dec} = -0.489 \times 10^{10}$ cm^{-2}. For the deuterated solvent the neutron scattering length density is $\rho_{d-dec} = 6.60 \times 10^{10}$ cm^{-2}. The mixtures have the solvent scattering neutron length density $\rho_{solv} = x\rho_{d-dec} + (1 - x)\rho_{dec}$, where x is the molar fraction of deuterated decane in the solvent. Mixtures with $x = 0$, 0.333, 0.667, and 1 were used for 40−40 and 40−80, whereas $x = 0$, 0.286, 0.644, and 1 were used for 12−48.

Stock solutions of the solvent mixture of decane were prepared gravimetrically. The stock solutions were used in order to ensure the same isotopic composition of all solutions and background solvents. For 40−40 and 40−80, solutions with nominal concentrations of 20 and 50 mg/mL were mixed. Samples with 10 and 5 mg/mL were prepared by dilution. For the 12−48, only 20 mg/mL solutions were used.

Small-Angle Neutron and X-ray Scattering. Neutron scattering experiments were conducted at the SANS facility at DR3 at Risø National Laboratory, Risø, Denmark.[39] Neutrons with wavelength 5.6 and 10 Å with a resolution $\Delta\lambda/\lambda = 0.22$ (fwhm) were used to cover the scattering vector range $q = 0.0037-0.26$ Å^{-1}. Three combinations of wavelength (λ) and sample-to-detector distance l were used (λ/l = 5.6 Å /1.1 m, 5.6 Å/3.0 m, and 10 Å/6.0 m). The samples were kept in Hellma quartz cells with a path length of 1 or 2 mm depending on the fraction of deuterated solvent. The isotropic two-dimensional scattering spectra were azimuthally averaged to obtain the intensity vs the modulus of the scattering vector, $q = 4\pi(\sin\theta)/\lambda$, where 2θ is the scattering angle. The data were background subtracted and converted to absolute scale by dividing by the scattering recorded for pure water in a cell with 1 mm path length. The data were furthermore normalized by the transmission, sample thickness, and polymer concentration.

The SAXS measurements were performed on the pinhole SAXS camera at Risø National Laboratory. The camera uses the Cu Kα radiation from a 18 kW Rigaku rotating anode operated at 12 kW. The radiation is monochromated by a flat graphite pyrolytic crystal, and the beam is collimated by three collinear square slits. The two-dimensional data sets were recorded using an image plate detector or a two-dimensional position sensitive gas detector. The sample was contained in a glass capillary with a diameter of 2 mm. The SAXS data were azimuthally averaged. The background measured with a capillary filled with pure decane was subtracted. No attempts were made to convert the SAXS data to absolute scale.

3. Experimental Results

Heat Treatment and Isotope Effects. As decane is a nonsolvent for PS at room temperature, it is necessary to heat treat the sample. The heat treatment should furthermore ensure that a frozen-in equilibrium structure for the micelles is obtained, as this gives reproducible samples. It should also be noted that a prerequisite for analyzing contrast variation data by simultaneous model fitting is that the micelles are identical independent of the contrast.

There are some reports on the heat treatment procedure of PS−PI copolymers in decane in the literature. Price et al.[40] investigated a PS−PI block copolymer with molecular weight 13 000−38 000 between 25 and 65 °C. The light scattering showed a substantial change between the two highest temperatures of, respectively, 55 and 65 °C. Bahadur et al.[41] used temperatures between 40 and 50 °C when dissolving PS−PI block copolymers with several different molecular weights in decane. All polymers had a molecular weight of the PI of 20 000, whereas the PS molecular weight varied between 9000 and 33 000. Higgins et al.[42] investigated a block copolymer with molecular weight 50 000−80 000 and used heat treatment up to 130 °C. McConnell et al.[43] used at heat treatment at 50 °C for a series of block copolymers with PS molecular weight from 8000 to 45 000 and PS molecular weights from 15 000 to 45 000. Iatrou et al.[11] studied super-H-shaped molecules with a linear central PS block and three identical PI blocks attached to each end. The molecular weight of the PS block varied between 8400 and 85 000, whereas the PI blocks had molecular weights in the range 10 000 to 18 000. The samples were heat treated at 70 °C for 1 h. This shows that a very broad variety of different treatments has been applied.

We decided to use a heat treatment procedure in which the samples were kept at 80−85 °C for at least 3 h in an oven. The samples were subsequently cooled slowly overnight by turning off the power to the oven. To reduce the possible influence of presence of oxygen, the samples were sealed in vial in which the air was exchanged by argon. Gel permeation chromatography in toluene showed no signs of degradation after the heat treatment. The first set of samples were prepared in only 0 and 100% decane-*d* at 20 mg/mL. SAXS data were recorded for these samples (Figure 1, parts a−c). The data for the 40−40 and 40−80 samples show large differences in micellar size in the two solvents, whereas the data for the 12−48 sample show that the micelles are identical in the two solvent. So for the two highest molecular weights there are some subtle isotope effects present, and the micelles are not frozen-in equilibrium structures.

The glass transition temperature of PS is known to increase with the molecular weight. For the 12−48 sample, the treatment presumably took place above the glass temperature of PS, whereas it was below for the 40−40 and 40−80 sample. It is therefore reasonable to connect the problems with this, although the glass temperature of PS in the PS domains surrounded by PI and by decane cannot be expected to be the same as in the bulk. We subsequently prepared a new set of samples at 20 mg/mL for the 40−40 and the 40−80 sample. They were heat treated for more than 3 h at 100−105 °C and cooled slowly to room temperature. The SAXS data for these samples showed that the micelles were identical in 0 and 100% decane-*d* (Figure 1, parts d and e). This indicates that the glass temperature of the PS domains are different in protonated and deuterated decane, however, as the glass transition temperature is exceeded for both solvents, equilibrium frozen-in micelles can be prepared. The micelles prepared in protonated decane by heating to 80 °C were almost identical to the equilibrium micelles, whereas those in decane-*d* were significantly larger. This suggests that the glass transition temperature is higher in decane-*d* as compared to protonated decane.

After this SANS data were recorded for these samples and additional samples with 28.6% and 64.4% decane-*d* were prepared by mixing the samples with 0 and 100% decane-*d* in appropriate proportions. The subsequent fitting of the data for the 40−40 and 40−80 sample by the models described in the next section, showed an excess of intensity at the intermediate contrasts. The cores contain a smaller fraction of solvent (15−20% of volume) and the excess of intensity can be explained by this solvent not being completely exchanged by bulk solvent in the mixtures. It was possible to model this by having an inner region of the spherical core with noninterchanged solvent. The fitting of the data showed that the region was smaller in protonated decane as compared to deuterated decane. In the former solvent

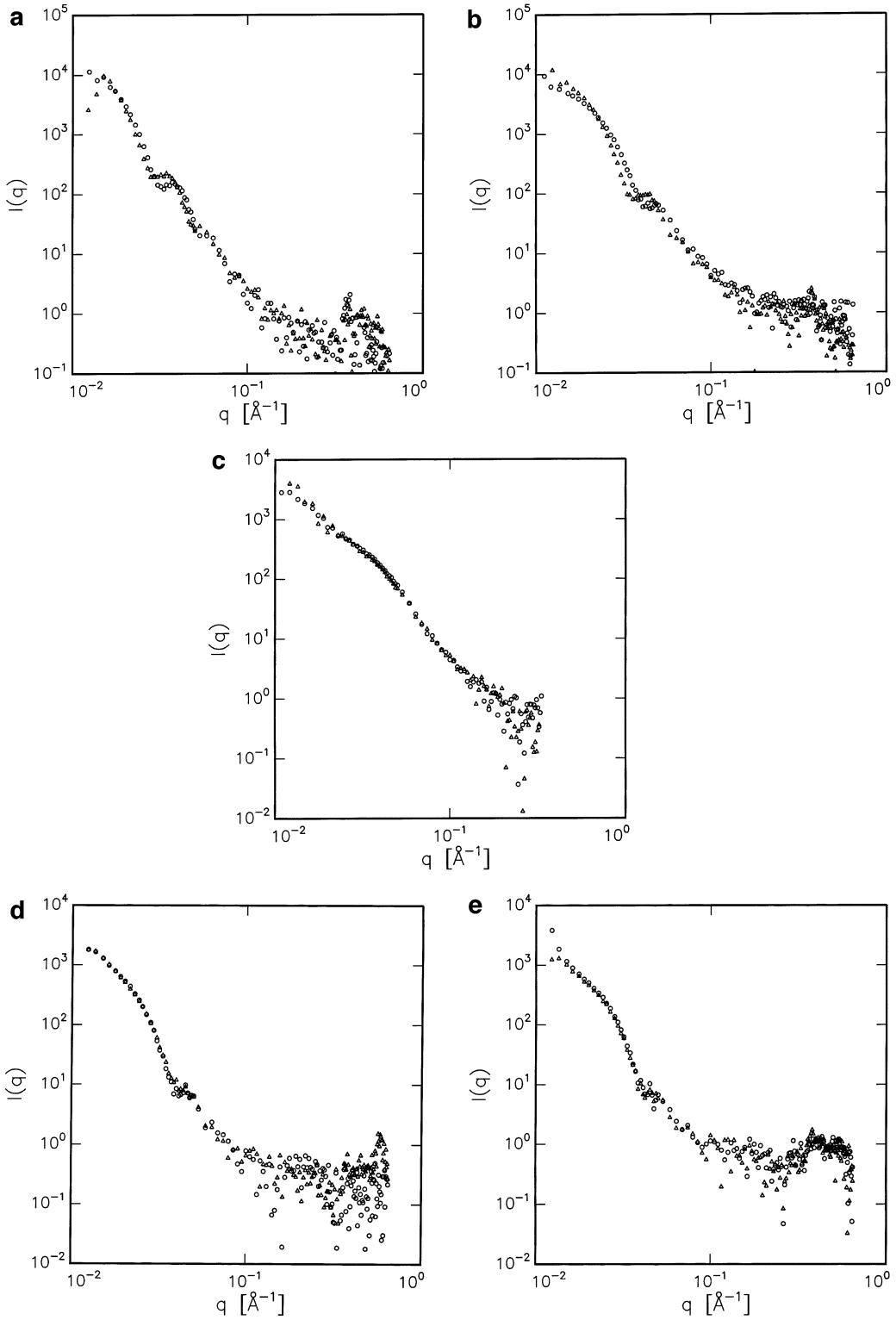

Figure 1. SAXS data for (a) 40−40, (b) 40−80, and (c) 12−48 in protonated and deuterated decane heated to 80 °C, respectively. (Note that the comparisons can only be considered qualitative, due to problems with the dynamic range of the image plate detector for these measurements). Data for (d) 40−40 and (e) 40−80 heated to 100 °C. Circles are for protonated decane (decane-*h*) and triangles are for decane-*d*.

it had a radius of 25−40 Å with a smooth profile and in the latter it had a radius similar to that of the core (105−115 Å) with only partial exchange close to the core surface. The immobility of the solvent for decane-*d* gives further support for the higher glass transition temperature in this solvent.

We found it unsatisfactory to have to include the noninterchanged solvent in our model as its presence could not be independently confirmed. We therefore decided to perform a new set of measurements on samples prepared with the actual mixtures of protonated and deuterated solvent as described in the previous section "Samples: Polymers and Solvents". SAXS measurements confirmed that the samples were identical in the different mixtures of decane and that the samples prepared at 20 and 50 mg/mL were identical.

The SANS contrast variation data for the three samples at 20 mg/mL are shown in Figure 2. Note that the data taken at different instrumental setting (sample−detector distances and wavelength) do not coincide in the overlap region due to the difference in instrumental smearing at the different settings. For the 40−40 and 40−80 sample, the data at 0, 33.3 and 66.7% show a peak at low scattering vectors q, which is due to intermicellar correlations. At high q, the data follow approximately a q^{-4} behavior at 0% and a $q^{-1.5}$ at 100%. The SAXS data for 0% decane-*d* are also shown in Figure 2. They look quite similar to the SANS data recorded in 0 decane, except that the slope a power-law scattering with a lower exponent is observed at high q.

In 0% decane-*d*, the PI blocks are almost completely matched and therefore only the scattering from the PS is observed. The q^{-4} behavior shows that the PS forms a compact, relatively homogeneous structure with sharp and well-defined interfaces. This is in agreement with the expectation that the PS forms the cores. At 100% decane-*d*, mainly the PI is observed. The lower exponent of the high-q power law is a signature of the diffuse and solvated character of the micellar corona, also in agreement with expectations. The lower-q behavior of the data in the Guinier region, where the initial sharp drop in intensity is observed demonstrates that the size of the micellar corona is much larger than the size of the core, showing that the PI corona surrounds the PS core.

4. Models

In the following the models used for fitting the experimental scattering data are described. A micellar model with noninteracting Gaussian chains and other models for interacting self-avoiding chains based on recent Monte Carlo simulation results are described. The inclusion of effects of size polydispersity and interparticle correlations in terms of a polydisperse hard-sphere model is also described.

Form Factor for Noninteracting Gaussian Chains. The form factor of a micelle contains four different terms: the self-correlation of the core, the self-correlation of the chains, the cross-term between the core and chains, and the cross-term between different chains. It can be written[10,17,25]

$$F_{\mathrm{mic}}(q) = N^2\beta_{\mathrm{core}}{}^2F_{\mathrm{core}}(q) + N\beta_{\mathrm{chain}}{}^2F_{\mathrm{chain}}(q) + 2N^2\beta_{\mathrm{core}}\beta_{\mathrm{chain}}S_{\mathrm{core-chain}}(q) + N(N-1)\beta_{\mathrm{chain}}{}^2S_{\mathrm{chain-chain}}(q) \quad (1)$$

where q is the scattering vector, N is the aggregation number of the micelle, and β_{core} and β_{chain} are the total excess scattering length of one PS block and one PI block, respectively. For a spherical homogeneous core with radius R and a smoothly decaying scattering length density at the surface, the core self-term can be written as

$$F_{\mathrm{core}}(q) = \Phi^2(qR)\exp(-q^2\sigma^2) \quad (2)$$

where $\Phi(y) = 3[\sin y - y\cos y]/y^3$ is the form factor amplitude of a sphere with a sharp surface. The last term takes into account a smoothly decaying density at the surface. σ describes the width of the interface.

The chain self-correlation term for the Gaussian chains with a radius of gyration R_g is given by the Debye function:

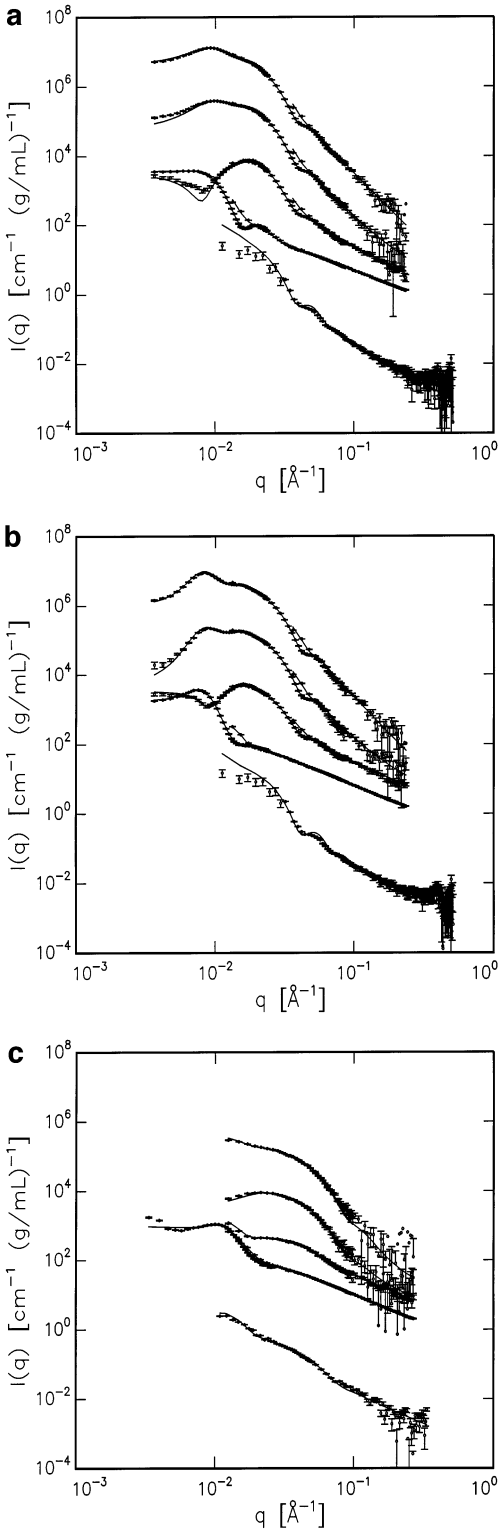

Figure 2. SANS contrast variation data and SAXS data for the three samples at 20 mg/mL. The four upper data sets for (a) 40−40 and (b) 40−80 are for 0, 33.3, 66.7, and 100% decane-*d*, respectively. For the 12−48 sample, these data sets are for 0, 28.6, 64.4, and 100%, respectively. The lower data set is the SAXS data. The four upper data sets are (from the top at high q) for 0, 33.3/28.6, and 66.7/64.4%, respectively, and they are multiplied by, respectively, 10^3, 10^2, and 10. The SAXS data set for 12−48 has been corrected for the problems with dynamic range, compared to the data in Figure 1. The lines are fits by the models described in the text. Note that the data and fits do not coincide in the overlap region of the data from different instrumental settings due to the difference in instrumental smearing.

$$F_{\text{chain}}(q) = \frac{2[\exp(-x) - 1 + x]}{x^2} \quad (3)$$

where $x = q^2R_g^2$.

The core-chain term is

$$S_{\text{core-chain}}(q) = \psi(qR_g)\Phi(qR)\exp(-q^2\sigma^2/2)\frac{\sin[q(d+R)]}{q(d+R)} \quad (4)$$

where $\psi(x) = [1 - \exp(-x)]/x^2$, again with $x = q^2R_g^2$. The chain−chain term is

$$S_{\text{chain-chain}}(q) = \psi^2(qR_g)\left(\frac{\sin[q(d+R)]}{q(d+R)}\right)^2 \quad (5)$$

In (4) and (5), $d \approx R_g$ as this mimics nonpenetration of the corona chains.

Form Factor for Interacting Self-Avoiding Chains. The expressions have been derived by Svaneborg and Pedersen[7] and are based on a Monte Carlo simulation study. The model has also in this case a homogeneous core; however, the chains are self-avoiding and interact mutually with a hard-sphere potential. The radius of the spheres on the chain is $\epsilon = 0.1b$, where b is the Kuhn length of the chains. The spheres on the chains interact also with a hard-sphere potential with the core. The simulations span a broad range of parameters (chain length, core radius, and surface coverage). It was shown that the form factor independent of the parameters can be written as

$$F_{\text{mic}}(q) = N^2\beta_{\text{core}}{}^2F_{\text{core}}(q) + N\beta_{\text{chain}}{}^2F'_{\text{eff}}(q) + 2N^2\beta_{\text{core}}\beta_{\text{chain}}S_{\text{core-chain}}(q) + N(N - F'_{\text{eff}}(q=0))\beta_{\text{chain}}{}^2S_{\text{chain-chain}}(q) \quad (6)$$

which contains the effective single-chain form factor

$$F'_{\text{eff}}(q) = \frac{F_{\text{exv}}(q)}{1 + \nu F_{\text{exv}}(q)} \quad (7)$$

where $F_{\text{exv}}(q)$ is the form factor of self-avoiding chains and ν is a parameter which increases with increasing concentration within the corona and is related to the chain−chain interaction within the corona. The expression[58] for $F_{\text{exv}}(q)$ is given in eq 13 of ref 33. The interference terms are, for a smooth core−corona interface

$$S_{\text{core-chain}}(q) = \Phi(qR)\exp(-q^2\sigma^2/2)A_{\text{chain}}(q)$$

and

$$S_{\text{chain-chain}}(q) = A_{\text{chain}}(q)^2 \quad (8)$$

where

$$A_{\text{chain}}(q) = \exp(-q^2\sigma^2/2)\left[4\pi\int \rho_{\text{chain}}(r)\frac{\sin(qr)}{qr}r^2\,dr\right] \Big/ \left[4\pi\int \rho_{\text{chain}}(r)r^2\,dr\right] \quad (9)$$

is the normalized Fourier transform of the configurationally average radial density distribution $\rho_{\text{chain}}(r)$ of the corona chains. The term $\exp(-q^2\sigma^2/2)$ in (9) takes into account the smooth variation of scattering length density at the core−corona interface.

In the present work, we used several different forms for $\rho_{\text{chain}}(r)$: (1) BoxGauss: A box function followed by a half Gaussian. (2) MaxEnt3: A maximum entropy based expression with three free parameters. (3) Spline2: The sum of two partial cubic *b* spline functions. (4) Spline3: The sum of three partial cubic *b* spline functions. (5) PowFix: A power law ($r^{-4/3}$) profile[9] with an empirical cutoff function. (6) PowFit: A power law profile with an arbitrary exponent and an empirical cutoff function. The first two are those used in ref 7. We decided to use several different forms in order to obtain estimates on the uncertainties on the determined $\rho_{\text{chain}}(r)$. The details of the profiles and on the calculation of the related scattering amplitudes are given in the Appendix.

The total neutron scattering lengths which are used in (1) and (6) are $\beta_{\text{core}} = \nu_{d-\text{PS}}(\rho_{d-\text{PS}} - \rho_{\text{solv}})$ and $\beta_{\text{chain}} = \nu_{\text{PI}}(\rho_{\text{PI}} - \rho_{\text{solv}})$, with $\nu_{d-\text{PS}} = \nu_{\text{Sty}}N_{\text{PS}}$ and $\nu_{\text{PI}} = \nu_{\text{iso}}N_{\text{PI}}$, where $\nu_{\text{sty}} = 166.1 \times 10^{-24}$ cm^3 is the styrene monomer volume, $\nu_{\text{iso}} = 121.4 \times 10^{-24}$ cm^3 is the isoprene monomer volume, and N_{PS} and N_{PI} are the polymerization indices of the PS and PI block, respectively. The total SAXS scattering lengths are calculated similarly from the excess electron densities, where excess means in excess of the electron density of the solvent. We want to allow for the presence of solvent in the core and therefore the volume of the core is given by $V_{\text{core}} = NV_{\text{PI}}/(1 - f)$, where f is the volume fraction of solvent in the core.

Size Polydispersity and Structure Factors. It was evident, when attempting to fit the data, that both size polydispersity and structure factor effects were present in the data. The structure factor effects can also be identified directly as peaks in the data at around $q = 0.01$ Å^{-1} in the 0 and 100% decane-*d* data in Figure 2. Even for samples with a relatively low volume fraction of polymers, the effects are quite pronounced due to the relatively extended and highly swollen corona chains. When structure factor effects are present in the contrast variation data, the effective structure factor, which one gets by dividing the intensity by the average form factor, depends on the actual contrast.[45] It is therefore very important that the structure factor effects are included as correctly as possible, which is done by the used of polydisperse structure models.[46] Such a structure factor model was used in the present work. Before describing the polydisperse model with structure factor effects included, it is useful to describe a monodisperse model with structure factor effects as this introduces the normalization and absolute scale employed in the fits.

The interaction potential is approximated by a hard-sphere potential. The corresponding hard-sphere structure factor[47] has previously been shown to give a good description of the structure factor of spherical micelles[18] and have been used in numerous cases (See, e.g.,[17,22,31,50−53]). An analytical expression for it can for example be found in ref 48. For the *monodisperse model* for block copolymer micelles the intensity has been shown to be given by[27]

$$I_{\text{mic}}(q) = F_{\text{mic}}(q) + A_{\text{mic}}(q)^2[S(q) - 1] \quad (10)$$

where $S(q)$ is the monodisperse hard-sphere structure factor and $A_{\text{mic}}(q)$ is the form factor amplitude of the radial scattering length distribution of the micelle.[27] For the micelles with noninteracting Gaussian chains it is

$$A_{mic}(q) = N\beta_{core}\Phi(qR)\exp(-q^2\sigma^2/2) + N\beta_{chain}\psi(qR_g)\frac{\sin[q(R+d)]}{q(R+d)} \quad (11)$$

For the micelles with interacting semiflexible chains it is

$$A_{mic}(q) = N\beta_{core}\Phi(qR)\exp(-q^2\sigma^2/2) + N\beta_{chain}A_{chain}(q) \quad (12)$$

The structure factor $S(q)$ used in (10) depends on two parameters, the hard-sphere interaction radius R_{hs} and the hard-sphere volume fraction η. Note that one can write $R_{hs} = R + \Delta R_{hs}$, where ΔR_{hs} is related to the width of the corona, i.e., $\Delta R_{hs} \approx 2R_g$.

The scattering cross section for the model in absolute units for data normalized by the concentration c is given by

$$\frac{1}{c}\frac{d\sigma(q)}{d\Omega} = \frac{I_{mic}(q)}{M_{mic}} \quad (13)$$

where M_{mic} is the mass of a micelle. It can be calculated as $M_{mic} = \rho_p N V_p$, where ρ_p is the specific density of the block copolymer, N is the aggregation number, and V_p is the volume of one polymer chain.

In the *polydisperse model*, a Gaussian number distribution for the core radii was assumed:

$$D(R) = \exp[-(R - \langle R\rangle)^2/\sigma_R^2]/(\sqrt{2\pi}\sigma_R) \text{ for } R > 0 \quad (14)$$

In this expression, $\langle R\rangle$ is the average radius and σ_R is the width of the distribution, which is truncated at $R = 0$. The micelles are assumed to have the same solvent fraction in the core, the same R_g of the coronal PI chains and the same radial coronal $\rho_{chain}(r)$ when the appropriate core radius R is used in the expressions.

The intensity has been shown to be given by[27]

$$I_{mic}(q) = \int F_{mic}(q, R)D(R)\,dR + \int\int A_{mic}(q, R)A_{mic}(q, R')[S(q, R, R') - 1]D(R)D(R')\,dR\,dR' \quad (15)$$

where $S(q, R, R')$ are partial structure factors. Also for the polydisperse model, we used a hard-sphere interaction potential. The intensity in (15) was calculated using the expressions of Vrij,[49] with the assumption that the hard-sphere radius has the following simple dependence on the core radius: $R_{hs}(R) = R + \Delta R_{hs}$. This expression is in agreement with the assumption that the corona profile has a constant thickness independent of R and only depends on R through the position of the core−corona interface. The model was included in the program for the fitting so that ΔR_{hs} and an effective polymer volume fraction η_{pol} were fitting parameters.

The scattering cross section of the model in absolute units for data normalized by the polymer concentration is

$$\frac{1}{c}\frac{d\sigma(q)}{d\Omega} = \frac{1}{\langle M_{mic}\rangle}I_{mic}(q) \quad (16)$$

where $\langle M_{mic}\rangle$ is the average micellar mass with respect to the distribution $D(R)$. It is given by

$$\langle M_{mic}\rangle = \rho_p\frac{4\pi}{3}(1-f)\int_0^\infty D(R)R^3\,dR \quad (17)$$

where it has been taken into account that a fraction f of the core volume is occupied by solvent.

When the models were fitted to the experimental data, the model scattering intensities (eqs 13 and 16) were smeared by the finite instrumental resolution.[54] For each setting the intensity was convoluted with the appropriate resolution function. Note that all four SANS contrast variation data sets (and the SAXS data when measured) were fitted simultaneously, with one structural model in which the contrast of the core and the chains were varied appropriately. Standard least-squares methods were applied for performing the fits.[55]

The fitting parameters depends on which model is considered. For the monodisperse model with noninteracting Gaussian chains, there are seven parameters: Aggregation number N, solvent volume fraction in the core f, radius of gyration of the PI chains R_g, displacement of the chains d, width of the core−corona interface σ, effective hard-sphere volume fraction η, and effective hard-sphere interaction radius R_{hs}. An overall scale factor was also used for fitting the SAXS data which are on an arbitrary scale. This gives five parameters for describing the micellar structure and two parameters for describing the interactions. For the corresponding polydisperse model, the number of fit parameters increase by only one, the width of the size distribution σ_R. Note that the hard-sphere radius is replaced by ΔR_{hs} and η by η_{pol}.

The polydisperse model with interacting chains with a box+half Gaussian coronal profile (BoxGauss) has seven parameters for describing the micellar structure (see the Appendix for details): $\langle R\rangle$, σ_R, f, R_g, ν, R_c, and s. The maximum entropy profile MaxEnt3 has eight parameters, (a_1, a_2, and a_3 instead of R_c and s), the profile with two partial b splines (Spline2) has seven parameters (a_1 and s instead of R_c and s), whereas the profile with three partial b splines (Spline3) has eight parameters (a_1, a_2, and s instead of R_c and s). The power-law profile with $r^{-4/3}$ (PowFix) has seven parameters for the profile, whereas the profile with an arbitrary exponent (PowFit) has eight parameters.

5. Results

We first fitted the data sets for 40−40 and 40−80 at 20 mg/mL by all models described in the previous section. The aim was to decide which one was the best-suited and to look for the variation in the results for the models providing the best fits, to obtain an estimate of the reliability of the results and the possible influence of the chosen parametrization for the radial profile. In the next step, we fitted the data for 40−40 and 40−80 for all concentrations as well as the data for 12−48 at 20 mg/mL by the best suited model, which turned out to be the one with three partial b splines. The models with noninteracting Gaussian chains and the monodisperse models with interacting chains did not provide satisfactory fits, so the results from fitting these models are not discussed further.

Comparison of Models. For the 40−40 sample, BoxGauss, MaxEnt3, Spline2, Spline3, and PowFit gave fits of similar quality. For the 40−80 sample, MaxEnt3, Spline2, Spline3, PowFix, and PowFit gave fits of similar quality. The curves in Figure 2, parts a and b, are fits for the Spline3 model, and the resulting profiles

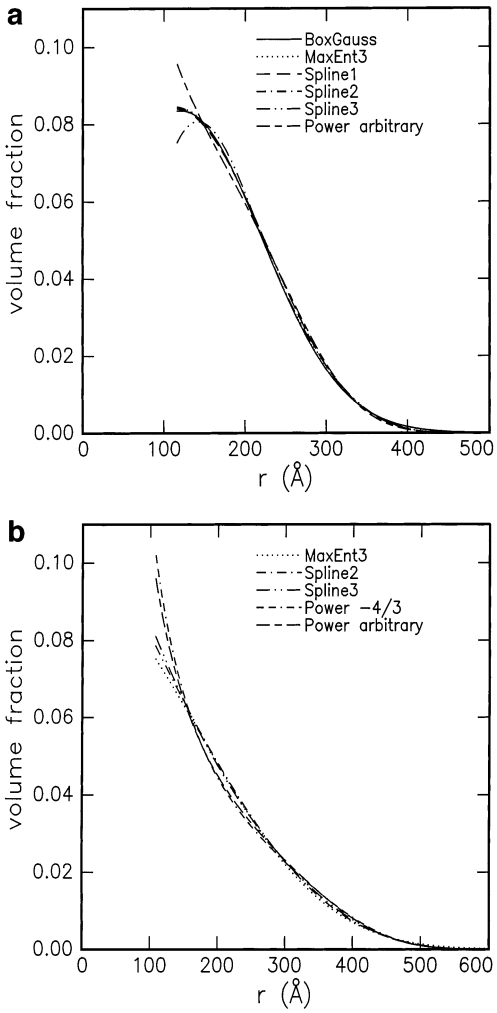

Figure 3. Radial profiles for the corona for models with interacting chains. Only the profiles for the best fits are shown: (a) 40−40; (b) 40−80.

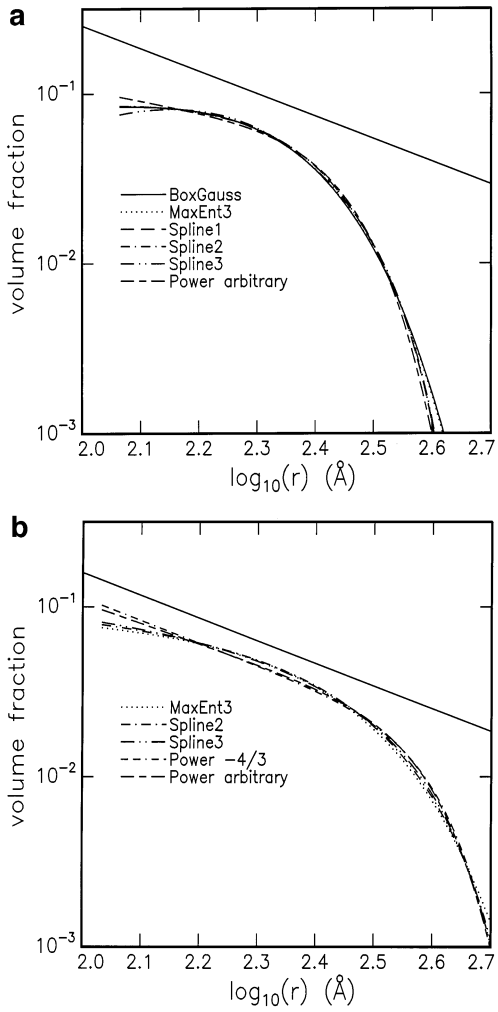

Figure 4. Same as Figure 3, but in double logarithmic presentation. A line with the slope $-4/3$ has been drawn for comparison.

are shown in Figure 3 in linear scales and in Figure 4 in a double logarithmic scales. The fit to the SAXS data were calculated using electron densities instead of scattering length densities and only an overall scale factor was fitted. The fits show very good agreement with the data for both samples. For 40−80 the agreement with the SANS data are nearly perfect for all contrasts, whereas some minor deviations are present for the SAXS data. The main deviations are at low q where the data are somewhat unreliable due to the subtraction of the background (parasitic scattering, scattering from capillary). For the 40−40 sample similar deviations are observed for the SAXS data. Minor deviations are also observed for the intermediate contrasts (33.3 and 66.7% decane-d) at low q. We believe that these deviations originate from from polydispersity of the width of the corona and from excess scattering due to correlation between molar mass of the blocks and the aggregation number of the micelle. A correlation of the latter kind could be that the block copolymers with the longest PI chains preferentially aggregate into the micelles with the lowest aggregation number, which have the largest curvature. This would provide more space for each chain and increase the configurational entropy of the chains. The consequence of such a preferential aggregation is that there is a composition variation with the aggregation number of the micelles. Such an effect gives extra scattering in the forward direction and in the minima of the scattering curves. The omission of this from the model could be the reason for the deviation between the model and the data for the intermediate contrast. We made attempts to model the effects of corona polydispersity and compositional variation and obtained improvements of the quality of the fits. However, there are many different ways of doing the modeling and as the influence on the result for the corona scattering (profile and effective single-chain scattering) was quite small, the results from fitting these models are not included in the present paper.

For the profiles displayed in Figure 4, the width of the corona for the sample with the largest molecular weight of the PI chains is as expected largest. For each of the samples the spread in the curves is modest except close to core surface where it is ±10%. There is a similar polymer volume fraction close to the core surface for the two samples, however, the shape of the profiles are quite different. For 40−40 it appears to be Gaussian-like, whereas it is more like a power law for the 40−80 sample. Figure 4 shows that for the 40−80 sample the profile is in agreement with a power-law behavior $r^{-\alpha}$ with an exponent of α in the range between 1 and $4/3$ from 100 to 300 Å. An exponent cannot be determined with any confidence for the 40−40 sample. The different functional behavior of the profiles are also reflected in the scattering data for the corona in 100% decane-d. For

Table 1. Parameters Related to the Effective Single-Chain Scattering, R_g and $F'_{eff}(0)$, for the Best-Fit Models to the 20 mg/mL Data for 40−40 and 40−80

40-40

	BoxGauss	MaxEnt3	Spline2	Spline3	PowFit
R_g (Å)	82.3	82.3	81.3	81.2	81.8
$F'_{eff}(0)$	0.297	0.300	0.316	0.302	0.331

40−80

	MaxEnt3	Spline2	Spline3	PowFix	PowFit
R_g (Å)	118.4	115.5	116.3	120.5	119.3
$F'_{eff}(0)$	0.335	0.355	0.359	0.357	0.364

40−40, which has a relatively compact form, there is a pronounced secondary maximum in the scattering data. In contrast, for 40−80, where the profile has a stronger decay, the secondary maximum is almost completely smeared out.

The two samples have a similar size of the core, $\langle R \rangle$ = 115 Å for 40−40 and 107 Å for 40−80, minor differences in polydispersity, σ_R = 14 Å for 40−40 ($\sigma_R/\langle R \rangle$ = 0.12) and 10 Å for 40−80 ($\sigma_R/\langle R \rangle$ = 0.093), and minor differences in solvent fractions in the core, f = 0.16 for 40−40 and 0.23 for 40−80. The repulsive interactions between the chains are most pronounced for 40−80, which has the longest chains. By having a larger amount of solvent in the core, the 40−80 micelles have more space for each chain and this increase the configurational entropy. Thus, the presence of more solvent in the core of the 40−80 micelles as compared to those of 40−40 is in agreement with our expectations. Note that the determined solvent fractions are influenced by possible systematic errors in the determination of the absolute scale, of the polymer concentration, and of the molar masses of the blocks. We estimate the (systematic) error on the values of f to be ±0.1.

The parameters, which can be expected to couple most strongly to the corona profile shape, are the other two parameters entering the corona scattering, the radius of gyration of the chains R_g and the effective forward scattering $F'_{eff}(0) = 1/(1 + \nu)$. These are given in Table 1. From the numbers one can estimate averages and uncertainties as R_g = 81.8 ± 0.5 Å and $F'_{eff}(0)$ = 0.31 ± 0.02 for 40−40 and R_g = 118 ± 3 Å and $F'_{eff}(0)$ = 0.35 ± 0.02 for 40−80.

The importance of chain-chain interactions can be estimated by calculating the reduced surface coverage $\Sigma - NR_g^2/(4[(R + R_g)]^2)$. The parameter is equivalent to a reduced concentration c/c^* for a semidilute solution, where c^* is the overlap concentration. The reduced surface coverage is derived by considering the projected surface area per chain (πR_g^2) relative to that available per chain in the middle of the corona, $4\pi(R + R_g)^2/N$.

For the Spline3 model, the aggregation number N is 79.5 for 40−40 and 51.4 for 40−80, which together with the values for R_g of 81.2 and 116.3 Å, respectively, and core radius, $\langle R \rangle$ = 115 and 107 Å, respectively, lead to reduced surface coverages of Σ = 3.4 and 3.5, respectively. So the values for the surface coverage do not justify the difference in the radial corona profiles, and it is thus relevant to consider other parameters, which characterize the structure and which are different for the two polymers. One such parameter is dimensionless curvature given by $\kappa = R_g/\langle R \rangle$, which is the natural parameter for characterizing the curvature of the surface relative to the width of the corona. The values for κ are, respectively, 0.70 and 1.10, and thus differ significantly. Therefore, the difference in curvature could provide an explanation of the difference shapes of the profiles. As the curvature effects are much larger for 40−80, this means that there is comparatively less space for the chains close to the surface and therefore the chain have to be more stretched in this case. This in turn leads to a less compact power-law-like behavior in the vicinity of the core surface.

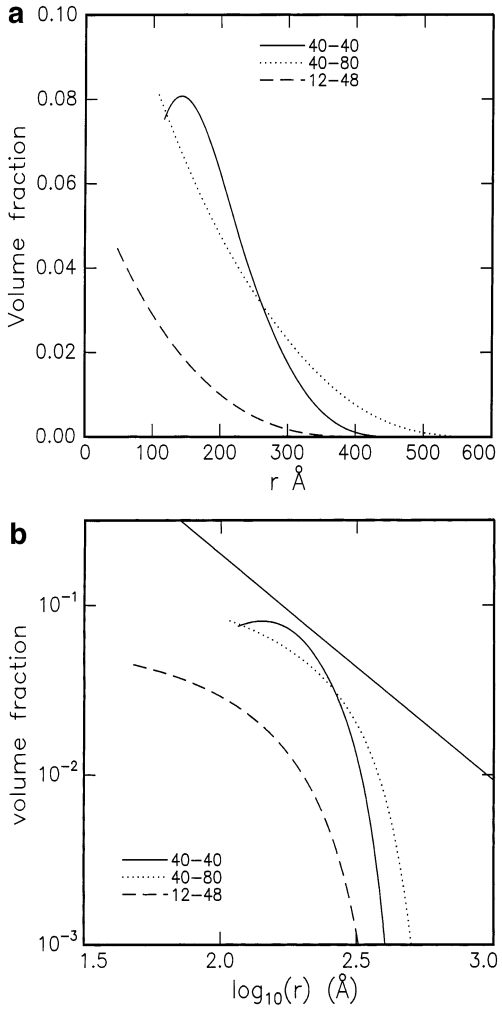

Figure 5. Radial profiles for the corona for the Spline3 corona model for 40−40, 40−80, and 12−48: (a) linear scales; (b) double logarithmic scales. A line with the slope $-4/3$ has been drawn for comparison.

The contrast variation SANS data and SAXS data for 12−48 for 20 mg/mL are shown in Figure 2c. The scattering intensity was relatively low and therefore the low-q part below 0.01 Å $^{-1}$ was only measured for the sample in 100% decane-d. Note that at this contrast, there is an increase in intensity at low q which might be due to the presence of some large-size objects. The curves in the figure are for the Spline3 model. The resulting profile is shown in Figure 5. It is strongly decreasing with increasing distance and similar to the profile for 40−80. This is also in agreement with the fact that a secondary maximum in the scattering data is not observed in 100 decane-d for these two samples. Considering the expected uncertainty of the profile, it is in agreement with a power-law behavior $r^{-\alpha}$ with a fairly low exponent of α = 0.7 in the range 50−200 Å.

For 12−48, the core radius is $\langle R \rangle$ = 48 Å and the polydispersity is σ_R = 8.1 Å ($\sigma_R/\langle R \rangle$ = 0.17). There is a large fraction of solvent in the core, f = 0.54, and the

aggregation number is only 12.5. The radius of gyration of the chains is $R_g = 79$ Å, and the forward scattering of the effective single-chain form factor is $F'_{eff}(0) = 0.45$. From these values, a reduced surface coverage and a curvature can be calculated to be $\Sigma = 1.2$ and $\kappa = 1.65$, respectively. From the Σ value, one should expect a weaker chain−chain interaction, than for 40−40 and 40−80 sample. However, the κ value is even higher than the value for 40−80, and therefore there is still a significant chain−chain interaction close to the surface, which leads to a strong stretching of the chain in this region.

Concentration Series. The contrast variation SANS data for 40−40 for 5, 10, and 50 mg/mL are shown in Figure 6, and the corresponding data for 40−80 are shown in Figure 7. Data for 20 mg/mL are shown in Figure 2, parts a and b. The data have been fitted by the Spline3 model, which in general was the model which provided the best fit to the 20 mg/mL data presented in the previous section. The fit to the 40−40 data are of high quality, however, with similar deviations at low q for the 66.7% decane-d data for all concentrations. As discussed in the previous section, these deviations are probably due to polydispersity of the corona width and correlation between molecular weight of the blocks and micellar aggregation number. For the 40−80 sample, the model gives an excellent fit to the data except for the highest concentration (50 mg/mL). This sample is very viscous, and the effective volume fraction of the micelles is so high that the sample is close to the liquid−solid transition of the micellar system. The data at the highest concentration are probably outside the range of validity of the hard-sphere model, which is also reflected by the fact that the model is not able to reproduce the sharp structure factor peaks in the data.

The radial profiles of the corona are shown in Figure 8, and the fit results for the model parameters are displayed in Table 2. The profile for the 40−40 sample show good agreement for the different concentrations with a spread of about 10% close to the core surface. All profiles show a relatively compact structure with indications of a small depletion close to the core surface. The profiles for the 40−80 display a larger spread and the one at the highest concentration is quite different from the rest. It is probable that the deficiencies of the structure factor model give rise to systematic errors in this profile. At the three lowest concentrations, the profiles have a strong decay in agreement with a power-law behavior, $r^{-4/3}$. Note that the corona width is smaller at the two highest concentrations, 20 and 50 mg/mL, which could be the result of intermicellar interactions. Such an effect is not observed for the 40−40 sample.

The fit results in Table 2 show that the micellar core size and aggregation numbers are independent of concentration. This is expected for the 5, 10, and 20 mg/mL data, as the 5 and 10 mg/mL samples were prepared by dilution of the 20 mg/mL sample. The 50 mg/mL sample were mixed at the actual concentration and the agreement of the data for this sample with the rest of the data demonstrates reproducibility and that the micelles can be considered as frozen-in equilibrium structures.

The average parameters are also listed in the table. The micelles are larger for 40−40 and the relative polydispersity is also larger for this sample, i.e., $\sigma_R/\langle R\rangle = 0.11$ as compared to $\sigma_R/\langle R\rangle = 0.086$ for the 40−80 sample. The results also show that the solvent volume fraction f is slightly larger for 40−80 than for 40−40.

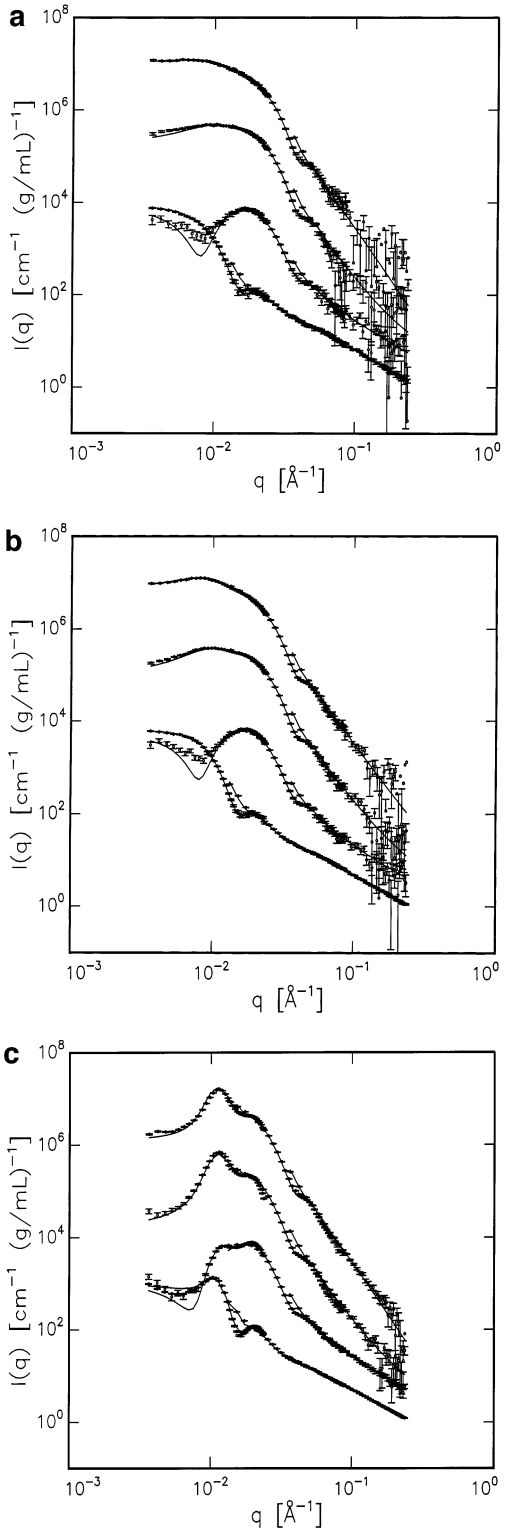

Figure 6. SANS contrast variation data for 40−40 at different concentrations. The four data sets in each plot are (from the top at high q) for 0, 33.3, 66.7, and 100% decane-d, respectively, and the data for 0, 33.3, and 66.7% are multiplied by respectively, 10^3, 10^2, and 10. Key: (a) 5, (b) 10, and (c) 50 mg/mL. Data for 20 mg/mL are shown in Figure 2.

The radius of gyration of the chains R_g are 78 ± 4 Å for 40−40 and 123 ± 9 Å for 40−80, which agree very well with literature values of 81 and 121 Å, respectively,[56] for PI in a good solvent. For the 40−40 sample,

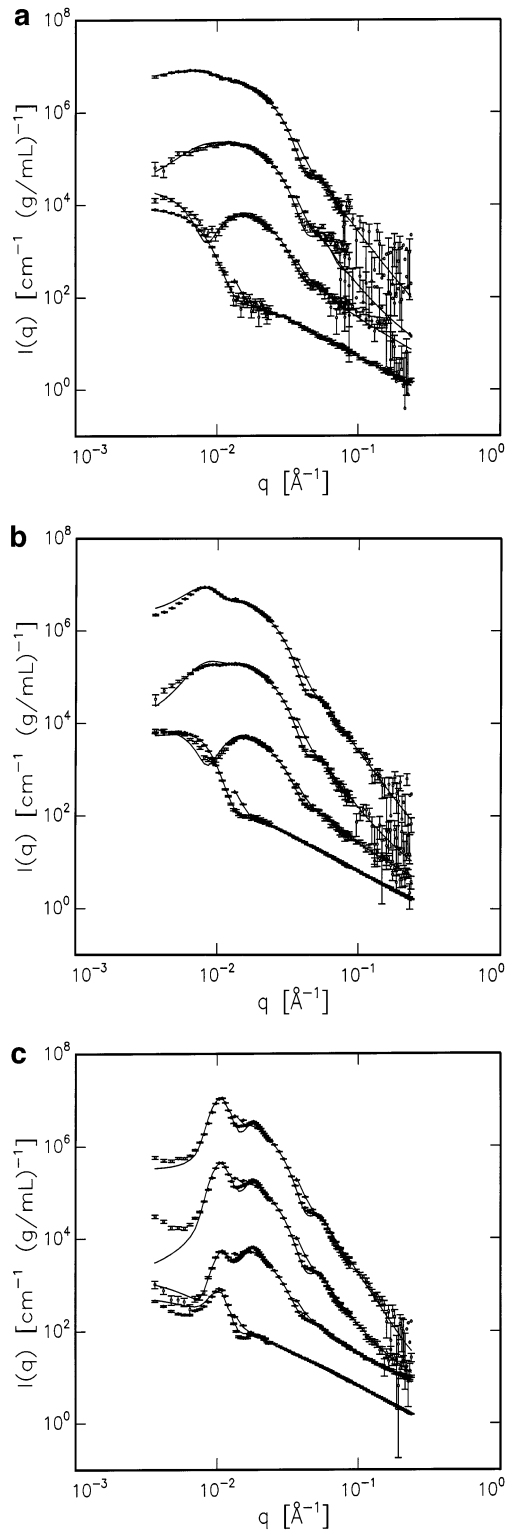

Figure 7. SANS contrast variation data and SAXS data for 40−80 at different concentrations. The four data sets in each plot are for 0, 33.3, 66.7, and 100% decane-*d*, respectively, and the data for 0, 33.3, and 66.7% are multiplied by respectively, 10^3, 10^2, and 10. Key: (a) 5, (b) 10, and (c) 50 mg/mL. Data for 20 mg/mL are shown in Figure 2.

the forward scattering of the effective single-chain scattering function $F'_{\text{eff}}(0)$ varies significantly and almost systematically with concentration. For 40−80, the values have a small spread and do not show a systematic variation with concentration. Note that the average value of $F'_{\text{eff}}(0)$ is, as expected, slightly lower for 40−80, which has a larger value of the reduced surface coverage Σ.

The fitted effective polymer volume fractions η_{pol} are determined from the structure factor effects. As the density of the two block copolymers are close to unity, the values are expected to be 0.005, 0.01, 0.02, and 0.05 for the polymer concentrations 5, 10, 20, and 50 mg/mL, respectively. For 5 and 10 m/mL, the η_{pol} values are somewhat larger, where as for 40−40, the value is slightly higher for 20 mg/mL and comparable for 50 mg/mL. For 40−80 the η_{pol} values are slightly smaller for 20 mg/mL and significantly smaller for 50 mg/mL.

A rough estimate of the hard-sphere volume fraction η_{hs} can be obtained from the values in the table as

$$\eta_{\text{hs}} = \frac{\eta_{\text{pol}} V_{\text{PS}}(\langle R\rangle + \Delta R_{\text{hs}})^3}{(1-f)V_{\text{pol}}\langle R\rangle^3} \tag{18}$$

where V_{PS} is the volume of the PS block and V_{pol} is the volume of the whole polymer. $V_{\text{PS}}/V_{\text{pol}} = 0.477$ for 40−40 and $V_{\text{PS}}/V_{\text{pol}} = 0.346$ for 40−80. The calculated values for η_{hs} are given in Table 2. They have been calculated using the average values of f, $\langle R\rangle$, and ΔR_{hs}. For 40−40, the values are in the range 0.0686−0.508, and therefore, the structure factor effects are important at all concentrations. The largest value at 50 mg/mL is close to the jamming transition of the monodisperse hard-sphere model. The values for 40−80 are large due to the larger extent of the corona and reach $\eta_{\text{hs}} = 0.704$ for 50 mg/mL. This value is outside the range of validity of the hard-sphere model and confirms that the sample is probably within the region where the micelles form a solid. Note that the structure factor peaks in Figure 7c, despite the high hard-sphere volume fraction, are not very sharp due to the presence of size polydispersity and instrumental smearing. For the 12−48 sample, $V_{\text{PS}}/V_{\text{pol}} = 0.165$ and $\eta_{\text{hs}} = 0.042$ for 20 mg/mL, so the interaction effects are comparatively smaller, which is probably due to the lower polymer density in the corona.

The range of the interaction potential is expected to be related to the width of the corona. Therefore, one expects $\Delta R_{\text{hs}} \approx 2R_{\text{g}}$. For 40−40 one has $\Delta R_{\text{hs}}/R_{\text{g}} = 2.39$, for 40−80 $\Delta R_{\text{hs}}/R_{\text{g}} = 2.16$, and for 12−48 $\Delta R_{\text{hs}}/R_{\text{g}} = 2.7$. These values are in reasonable agreement with those expected.

6. Monte Carlo Simulations

The model fits have provided estimates of various parameters of the micelles like core radius, number of chains, radius of gyration and $F'_{\text{eff}}(0)$, the value of the effective chain form factor in the forward direction. This allows a comparison of $F'_{\text{eff}}(0)$ and the radial profile of the corona $\rho_{\text{chain}}(r)$ with those obtained by Monte Carlo simulations.[5−7] However, these simulations, although spanning a broad range of the parameter space were performed for relative short chains in terms of contour length relative to the Kuhn length and a direct comparison is not possible. We have therefore performed a new set of simulations for parameter values estimated in the analysis of the experimental data described in the previous section.

The simulation model consists of semiflexible chains grafted to a hard sphere, which represents the core. The chains in the model has a fixed valence angle, free rotation around the bonds, and a constant distance between the points on the chains.[5−7] Spheres of radius $\epsilon = 0.1b$ are placed at each point along the chain and

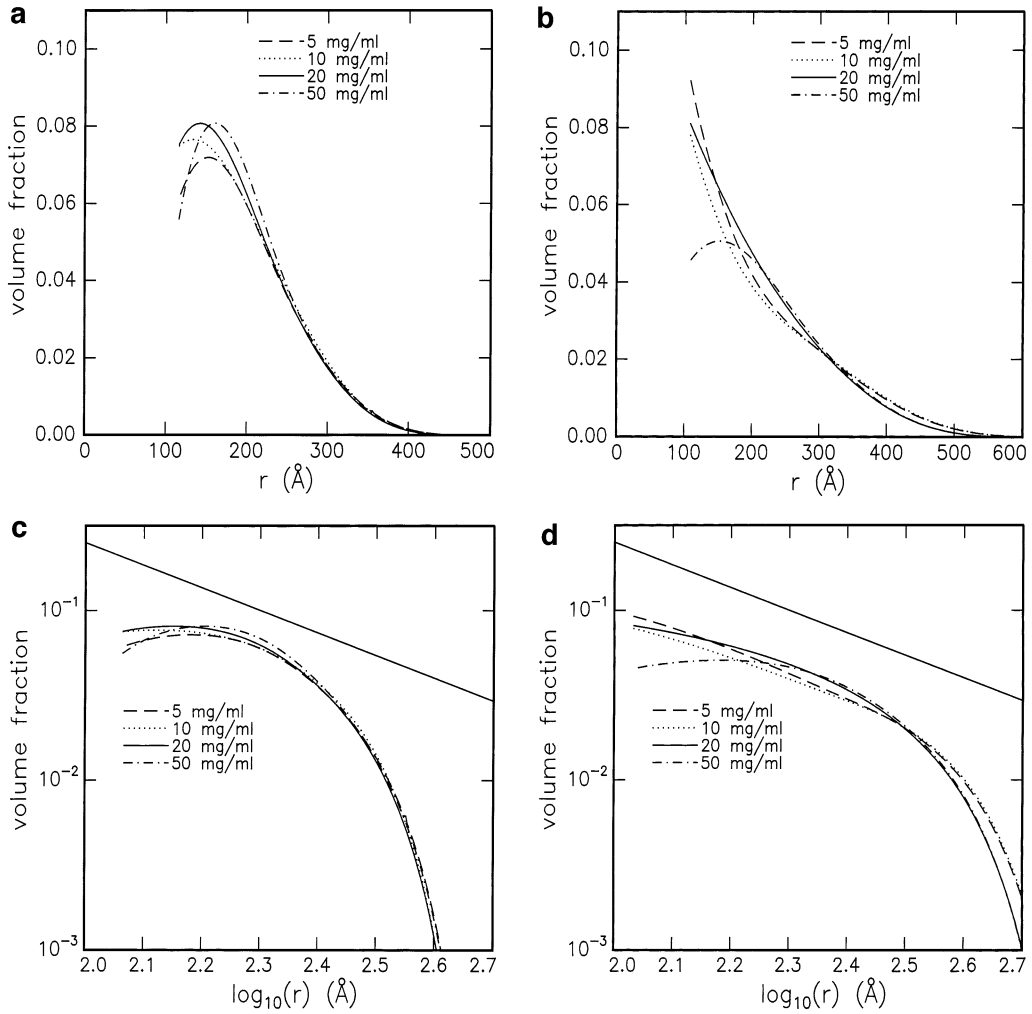

Figure 8. Radial profiles for the corona for Spline3 corona model for 40−40 and 40−80 for different concentrations: (a, b) linear scales; (c, d) double logarithmic scales. A line with the slope $-4/3$ has been drawn for comparison.

these interact through a hard-sphere potential with each other and with the core. The particular value of ϵ gives excluded volume interactions with a strength similar to that found in real systems. In the previous simulations a value of the valence angle that gives six spheres per Kuhn length b and a sphere radius of 0.6 times the bond length were used. To have long chains with contour length of many Kuhn lengths we have used a sightly modified version of the model we have used previously.[5,6,7] The valence was chosen as $\theta = \pi/2$, which gives a Kuhn length of only one bond length. By the choice of valence angle, we limit the total number of spheres in the simulations, and it is possible to perform simulations for model structures corresponding to those found experimentally. More details on the simulations can be found in refs 5−7.

The parameters for the simulations are estimated from the fit results for the experimental data. For long chains, one has $R_g^2 = Nb^2/6$, when neglecting excluded volume interactions. For 12−48 and 40−40, R_g is about 80 Å and with an estimated Kuhn length of $b = 10$ Å[57] this gives $N = 384$. For 40−80 $R_g = 120$ Å which corresponds to $N = 864$. For the simulations of the 12−48 micelles, we used a core radius of $R = 50$ Å and had 12 chains on the surface. For 40−40, we used $R = 110$ Å and 80 chains on the surface, whereas for 40−80, $R = 100$ Å and 52 chains on the surface.

The radius of gyration of the individual chains, their scattering function $F_{chain}(q)$, the chain−chain ($S_{chain-chain}(q)$) and core-chain scattering function ($S_{core-chain}(q)$) and the total scattering function of the corona ($F_{corona}(q)$) were sampled during the simulations. The sampled R_g values are 91.87 ± 0.07 Å, 96.10 ± 0.07 Å, and 149.6 ± 0.1 for the 12−48, 40−40, and 40−80 simulations, respectively, so they deviate slightly from the experimental values due to the neglect of excluded volume interactions when estimating the chain length. From the R_g values, one can determine the reduced surface coverage and the curvature parameter. They are given in Table 3 together with the experimental values. There is a reasonable agreement between the two sets of values, although the curvature parameter is slightly larger for the simulations.

The total corona scattering functions are shown in Figure 9, and the radial profiles of the corona are shown in Figure 10. For the 12−48 and 40−80 simulations the scattering functions display a monotonic decrease as a function of increasing scattering vector modulus with only a weak indication of a secondary maximum. In contrast, the 40−40 simulation results display a clear secondary maximum. This difference reflects a difference in the radial profile (Figure 10). For the 40−40 simulation, the profile is relatively compact, whereas for the 12−48 and 40−80 simulations it is less compact and in a small range is in reasonable agreement with a power-law behavior with an exponent of -1.0 to $-4/3$. Figure 9 also contains the experimental corona scattering profiles for the 20 mg/mL samples. The structure

Table 2. Fit Results for the Spline3 Model

	c (mg/mL)				
	5	10	20	50	av
			40-40		
			Experimental		
η_{pol}	0.006 59	0.0115	0.0210	0.0488	
$\langle R \rangle$ (Å)	116.2	114.6	114.5	115.7	115 ± 1
σ_R (Å)	12.0	13.4	14.4	13.7	13 ± 1
f	0.209	0.154	0.157	0.146	0.17 ± 0.02
ΔR_{hs} (Å)	179	187	192	188	187 ± 5
R_g (Å)	73	81	81	77	78 ± 4
$F'_{eff}(0)$	0.70	0.52	0.30	0.37	0.47 ± 0.1
			Calculated		
N	78.0	79.9	79.5	83.1	80 ± 1
Σ	2.9	3.4	3.4	3.3	3.3 ± 0.2
η_{hs}	0.0686	0.120	0.219	0.508	
			40−80		
			Experimental		
η_{pol}	0.006 31	0.0137	0.0183	0.0370	
$\langle R \rangle$ (Å)	107.0	106.8	106.7	109.0	107 ± 1
σ_R (Å)	9.2	9.7	9.8	8.3	9.3 ± 0.8
f	0.186	0.196	0.225	0.292	0.23 ± 0.03
ΔR_{hs} (Å)	269	267	282	244	266 ± 15
R_g (Å)	125	137	116	115	123 ± 9
$F'_{eff}(0)$	0.35	0.32	0.36	0.27	0.33 ± 0.03
			Calculated		
N	55.3	55.3	51.4	52.8	54 ± 1
Σ	4.0	4.4	3.5	3.5	3.9 ± 0.4
η_{hs}	0.120	0.261	0.348	0.704	

Table 3. Reduced Surface Coverage and Curvature Parameter from Experiments (expt) and Simulations (sim)[a]

sample	Σ(expt)	Σ(sim)	κ(expt)	κ (sim)
12−48	1.2	1.13	1.65	1.83
40−40	3.4	3.55	0.70	0.87
40−80	3.5	3.54	1.10	1.36

[a]The experimental values are those determined for the 20 mg/mL sample (Table 1).

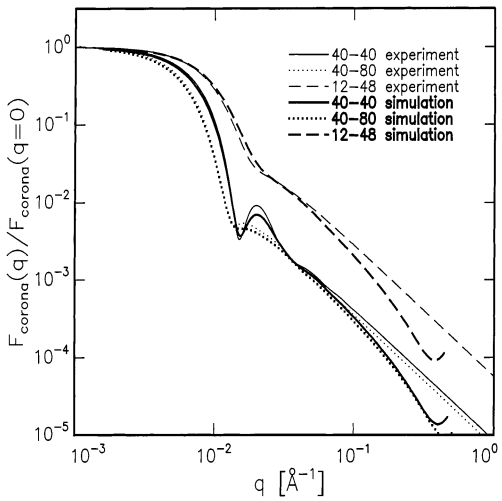

Figure 9. Comparison of corona scattering form factor from simulations and experiment for the micelle parameters determined from the experimental data.

factor effects have been eliminated and the calculations are for the average-size micelles. All data are normalized to unity for $q = 0$ and the simulation data have been scaled to give the best agreement with the experimental data in the low- and intermediate q regime. The rescaling corresponds to a Kuhn length of about 10 Å for the PI in agreement with previously published

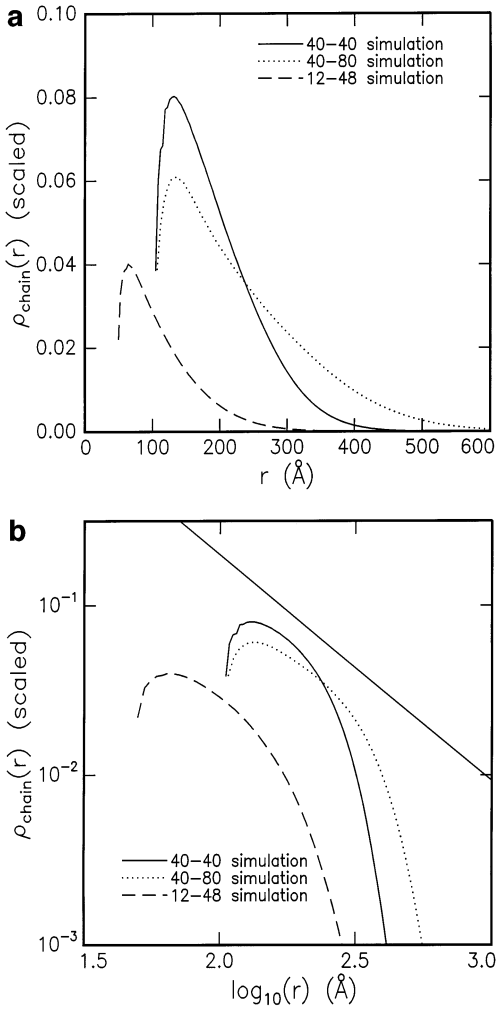

Figure 10. Radial profiles from the Monte Carlo simulations for the micelle parameters determined from the experimental data: (a) linear scales; (b) double logarithmic scales.

values.[57] Also, for the experimental data, it is only for the 40−40 data that clearly secondary maximum can be observed. The simulated and experimental data agree very well up to a q value of about 0.07 Å^{-1}. The experimental data display a power-law behavior for higher q values, whereas the simulation data display a behavior that is an artifact related to the local structure in used for describing the chains. This discretization error arises from the use of only one sphere/segment per Kuhn length.

The value of the effective form factor in the forward direction can be determined as described in ref 7 from a self-consistent analysis of the sampled contributions to the scattering function. One has from (6)

$$F_{corona}(q) = \beta_{chain}{}^2[NF'_{eff}(q) + N(N - F'_{eff}(q=0))S_{chain-chain}(q)] \quad (19)$$

with the effective single-chain form factor 7. The function $F_{exv}(q)$ entering $F'_{eff}(q)$ and the function $S_{chain-chain}(q)$ are known from the simulation, so only the forward value $F'_{eff}(q = 0)$ has to be determined by fitting expression 19 to the directly sampled function. For the three simulations, the fits gave $F'_{eff}(0)(q = 0) = 0.619 \pm 0.002$, 0.378 ± 0.001, and 0.356 ± 0.001 for the 12−48, 40−40, and 40−80 simulation, respectively. For the 20 mg/mL samples and the Spline3 fit, the corre-

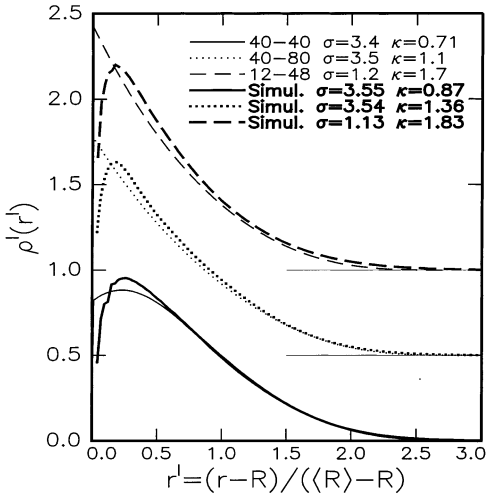

Figure 11. Comparison of rescaled radial profiles from simulations and experiment. The 40−80 and 12−48 profiles are shifted vertically by 0.5 and 1.0, respectively. The zero intensity lines are indicated at large r'.

sponding values are, respectively, 0.45 ± 0.02, 0.30 ± 0.02, and 0.36 ± 0.02, which are relatively close and show the same trend as the values obtained from the simulation results. The forward scattering can also be calculated using the scaling behavior (eq 26 in the Appendix) determined in the previously published simulation, which, however, are for shorter chains and lower curvatures. This gives 0.371, 0.219 and 0.214, respectively, which are somewhat lower than the values found experimentally and the values determined from the simulations for longer chains for coronas with larger curvatures.

The simulation radial profiles of the corona can also be compared directly to those determined from the experimental data. To compensate for small differences in the parameters describing the profiles, we compare the reduced profiles which are defined as

$$\rho'(r') = \rho_{\text{chain}}(r')/\int \rho_{\text{chain}}(r')\, \mathrm{d}r' \qquad (20)$$

where the reduced radial distance is defined as

$$r' = (r - R)/(\langle r\rangle - R) \qquad (21)$$

with $\langle r\rangle = 4\pi \int r \rho_{\text{chain}}(r) r^2\, \mathrm{d}r$.

The reduced radial profiles from simulations and experiments are displayed in Figure 11. The agreement is in general very good except very close to the core surface, where all simulation profiles show a narrow depletion layer. The contribution of this layer to the normalization integral is significant and therefore the scaled profiles are higher than the experimental profiles for $r' > 0.25$ for the 40−80 and 12−48 simulations.

The combination of scattering experiments and Monte Carlo simulations and the good agreement between the scattering form factors from the two approaches, offers a unique possibility to display the real-space structure of the micelles. This is due to the fact that in the Monte Carlo simulations the coordinate of all the spheres making up the micelles are available, and it is therefore possible to make three-dimensional drawings of representative structures for the micelles in the samples of PS−PI block copolymers in decane. The micelles generated from the Monte Carlo simulation coordinates are shown in Figure 12. The coronas give the impression of being quite dilute and very inhomogeneous with large fluctuations. It is therefore not surprising that the scattering from such structures cannot be generated by centrosymmetric models.

7. Summary and Conclusions

Contrast variation small-angle neutron scattering in combination with small-angle X-ray scattering have been employed in a detailed study of the structure and interactions of block copolymer micelles. A system consisting of polystyrene−polyisoprene block copolymers in decane was chosen, as this system has already been studied in some details by other groups (see, e.g., refs 11 and 40−43). The facts that decane is a strongly selective solvent for PI and that it is possible to obtain polymer blocks of relatively high molecular weights were also exploited, as these two aspects are relevant for obtaining a strong interaction between the chains in the corona of the micelles.

In the current study three samples of *d*-PS−PI have been investigated. For these samples, the contour length L of the solvated PI chains is much larger than the Kuhn length b and thus the chains are well within the flexible polymer region $L \gg b$. The SANS contrast variation data were analyzed together with small-angle X-ray scattering data using scattering functions recently derived from Monte Carlo simulations for a model with a spherical core and a corona of semiflexible chains interacting with a hard-core potential.[7] The analysis of the SANS data was performed on an absolute intensity scale and provided information on aggregation number and solvent fraction in the core. The latter was 15−20% for the 40−40 and 40−80 sample and even higher for the 12−48 sample, which has a low mass of the PS blocks in the core. As mentioned in section 3, the presence of solvent in the core was confirmed by the analysis of a series of measurements for which the intermediate contrast samples were prepared by mixing samples with 0 and 100% deuterated decane. The analysis showed that the solvent was bound to some extent and only slowly exchanged with the bulk solvent.

Small-angle X-ray scattering proved to be a very important tool to check for isotope effects and for ensuring that the samples prepared in different mixtures of protonated and deuterated solvent could be analyzed simultaneously. The study also showed that it was necessary to heat the samples with large molecular weights of the PS blocks in the cores (40−40 and 40−80) to quite high temperatures (∼100 °C) in order to get reproducible micellar structure independent of the deuteration of the solvent. That "equilibrium frozen-in" structures were obtained was supported by the fact that identical micelles were obtained for the stock solutions prepared with 20 and 50 mg/mL, respectively.

The analysis of the experimental data provides information on shape, aggregation number, polydispersity, core size, core solvation, and corona shape/size and on the interactions between the chains in the corona, which are significant for these micelles. The study showed that the shape of the corona profile depends on essentially two parameters: a reduced surface coverage of the corona chains, i.e., concentration relative to chain overlap concentration, and a curvature parameter, which is the width of the corona relative to the core radius. The three investigated samples turned out to span the parameter space reasonably with relatively large variations of reduced surface coverage as well as

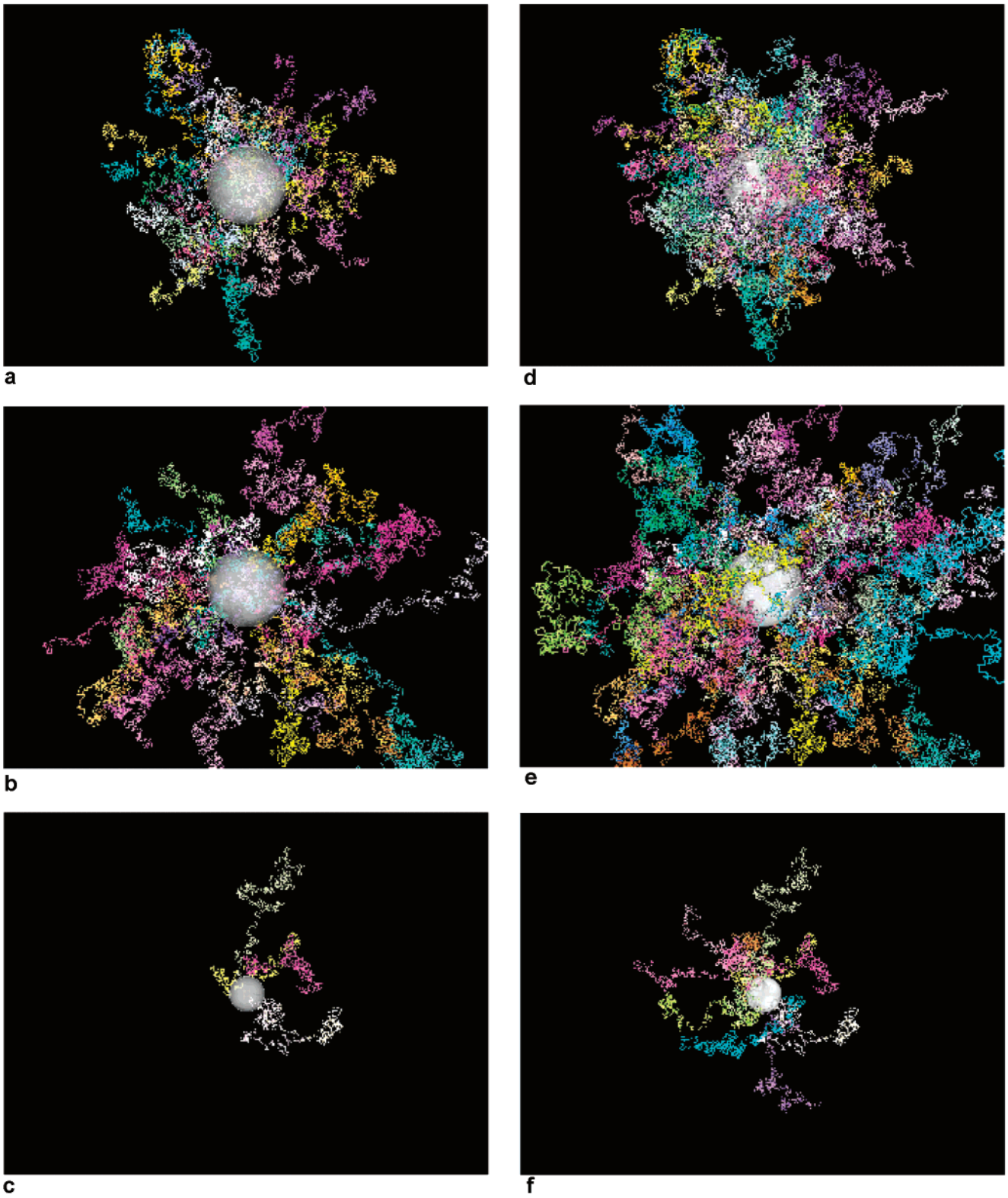

Figure 12. Representative structures for the block copolymer micelles generated by Monte Carlo simulation: (a and d) 40−40; (b and e) 40−80; (c and f) 12−48. For the structures shown in parts a−c, only half of the core is shown and only the chains attached to this half are displayed. In parts d−f, the full structures with all chains are displayed. The chains are represented by the spheres making up the excluded volume and sticks connecting the points along the chains.

curvature. For high curvatures the profile is in agreement with a power-law behavior as predicted by scaling theory.[9] For low curvatures the profile is more compact. The results are in agreement with previous literature reports.[35−37]

Comparisons of results for different parametrizations of the radial profiles of the corona and of results for different polymer concentrations were used to estimate errors on structural parameters as well as on the radial corona profiles. This was a very useful approach. It can in this connection be mentioned that the profiles based on cubic *b* splines are well suited for parametrizing the profiles and for varying the number of fit parameters used for describing the profile. This profile is further-

more quite easy to implement as closed form expressions are available. It could also be used to improve the original model for block copolymer micelles with noninteracting Gaussian corona chains[25] as core penetration of the chains is prohibited with such a parametrization of the radial profile.

The model used in the analysis also gives information on the reduction of the forward scattering of the single chain form factor for the corona chains due to the chain−chain interaction effects. The values are in general lower than the "universal" curve previously determined by Monte Carlo simulations.[6,7] This is probably due to the fact that the curvatures for the PS−PI micelles are larger than those in the simulation study and that the coronal chains are considerably longer for the PS−PI micelles than those in the simulation study. It should be noted that the simulation results also deviated from the universal curve for large curvatures, however, it would be interesting to perform simulations for micellar models with varying curvatures for long chains, although such simulations are extremely time-consuming due to the large number of degrees of freedom in the models in the relevant region of parameter space.

The measured scattering curves and the derived profiles are very well reproduced by the direct Monte Carlo simulations based on the parameters for the structures determined in the analysis of the experimental scattering data.

Advanced modeling in combination with contrast variation measurements is the ideal approach for determining the radial profile of the conona chains of block copolymer micelles. The form factor of the micelles can be written as

$$F_{\mathrm{mic}}(q) = N^2\beta_{\mathrm{core}}{}^2F_{\mathrm{core}}(q) + N^2\beta_{\mathrm{chain}}{}^2S_{\mathrm{chain}}(q) + 2N^2\beta_{\mathrm{core}}\beta_{\mathrm{chain}}S_{\mathrm{core-chain}}(q) \quad (22)$$

where a total scattering function of the corona $S_{\mathrm{chain}}(q)$ has been introduced, which includes both the effective single chain scattering and the chain−chain term. By performing the contrast variation measurements for at least three different contrasts, the three terms in (22) can be determined. The core-chain cross term $S_{\mathrm{core-chain}}(q)$ is the product of the core form factor amplitude and the corona scattering amplitude. The latter is directly the Fourier transform of the radial profile of the corona (eq 9), and therefore, the radial corona profile can (in principle) be determined by an inverse Fourier transformation of the cross term divided by the core form factor amplitude. The use of contrast variation is therefore equivalent to determining the phases of the amplitude of the corona scattering. Once the corona scattering amplitude and the aggregation number is known, it is obvious that information on the effective single chain form factor can be obtained from the total scattering function of the corona $S_{\mathrm{chain}}(q)$. In practice, the limitations are the finite q range of the data, counting statistics, polydispersity effects, structure factor effects, and instrumental smearing of the data.

Acknowledgment. The neutron scattering experiments reported in this paper were performed at the DR3 reactor at Risø National Laboratory and supported by the Commission of the European Community through the Training and Mobility of Researchers Program (TMR). I.W.H. acknowledges the support of the Engineering and Physical Sciences Research Council (U.K.). This work was supported in part by the Danish Natural Science Research Council.

Appendix: Models for the Corona Profile

In the following the different forms for $\rho_{\mathrm{chain}}(r)$ used in the analysis of the data are described. They are as follows. (1) BoxGauss: A box function followed by a half Gaussian. (2) MaxEnt3: A maximum entropy based expression with three free parameters. (3) Spline2: The sum of two partial cubic *b* spline functions. (4) Spline3: The sum of three partial cubic *b* spline functions. (5) PowFix: A power law ($r^{-4/3}$) profile[9] with an empirical cutoff function. (6) PowFit: A power law profile with an arbitrary exponent and an empirical cutoff function. The two first are those used in ref 7. The calculations of the related scattering amplitudes are also described.

The *BoxGauss* profile has the box part between R and R_c followed by the half-Gaussian with the width given by s, so that the profile is

$$\rho_{\mathrm{chain}}(r) = 0 \quad \text{for } r < R$$

$$\rho_{\mathrm{chain}}(r) = 1 \quad \text{for } R \le r < R_c, \quad \text{and}$$

$$\rho_{\mathrm{chain}}(r) = \exp[-(r - R_c)/(2s^2)] \quad \text{for } r \ge R_c \quad (23)$$

These expressions lead to

$$A_{\mathrm{chain}}(q) = \frac{S_g(q) + V(R_c)\Phi(qR_c) - V(R)\Phi(qR)}{V_0 + V(R_c) - V(R)}\exp(-q^2\sigma^2/2) \quad (24)$$

where the last term again takes into account the smoothness of the core−corona intelrface. $V(R) = 4\pi R^3/3$, $V_0 = 2\pi[4R_cs^2 + \sqrt{2\pi}(R_c^2 + s^2)s]$, and

$$S_g(q) = \frac{4\pi s^2\sin(qR_c)}{q} + \frac{2\pi s}{q}[\sqrt{2\pi}\exp(-q^2s^2/2)(qs^2\cos(qR_c) - R_c\sin(qR_c)) + 2\sqrt{2}D(qs/\sqrt{2})(R_c\cos(qR_c) - qs^2\sin(qR_c))] \quad (25)$$

The function $D[y] = \exp(-y^2)\int_0^y \exp(t^2)\,dt$ is the Dawson integral for which a numerical expression is given in ref 44. In the simulations it was found that that $|R - R_c| \approx 0$ and $s \approx R_g$ and that the concentration parameter in (7) follows approximately

$$\nu \approx 1.4\Sigma^{1.04} \quad (26)$$

where $\Sigma = NR_g^2/(4[(R + R_g)]^2)$ is the reduced surface coverage.

The *MaxEnt3* profile is given by

$$\rho_{\mathrm{chain}}(r) = 0 \text{ for } r < R$$

$$\rho_{\mathrm{chain}}(r) = \exp[-a_1(r - R) - a_2(r - R)^2 - a_3(r - R)^3] \quad \text{for } r \ge R \quad (27)$$

where a_1, a_2, and a_3 are parameters which gives the shape of the profile. The MaxEnt3 profile was Fourier transformed numerically using two different simple box integration schemes with (i) 100 points between R and $R + 5R_g$ and (ii) 500 points between R and $R + 6R_g$. We

did not find any difference in the fits performed by these two sets of parameters.

For the *Spline2* the radial density is given by a linear combination of the following two expressions:

$$\rho_1(r) = [4(r - R - s)^3 - (r - R - 2s)^3]/(4s^3) \quad \text{for } R \le r < R + s$$

$$\rho_1(r) = -(r - R - 2s)^3/(4s^3) \quad \text{for } R + s \le r < R + 2s$$

$$\rho_1(r) = 0 \quad \text{elsewhere} \tag{28}$$

and

$$\rho_2(r) = -(r - R - s)^3/(4s^3) \quad \text{for } R + s \le r < R+2s$$

$$\rho_2(r) = 0 \text{ elsewhere} \tag{29}$$

The parameter s gives the width of the profile. In the terminology of spline functions, s is the distance between the knots. The total profile is

$$\rho_{\text{chain}}(r) = [\rho_1(r) + a_1\rho_2(r)]/(1 + a_1) \tag{30}$$

where a_1 is a fitting parameter. The Fourier transform of the two contributions can be calculated separately. The first term is

$$A_1(q) = C_{\text{norm},1}[24\cos\{q(R + 2s)\}/q^6 + 6(R + 2s)\sin\{q(R + 2s)\}/q^5 - 96\cos\{q(R + s)\}/q^6 - 24(R + s)\sin\{q(R + s)\}/q^5 + 4(q^4Rs^3 + 3q^2Rs + 18)\cos(qR)/q^6 - 2\{2q^2s^3 - 9(R - 2s)\}\sin(qR)/q^5] \tag{31}$$

where

$$C_{\text{norm},1}{}^{-1} = s^4(15R^2 + 14Rs + 5s^2)/5 \tag{32}$$

The other contribution is

$$A_2(q) = C_{\text{norm},2}[24\cos\{q(R + s)\}/q^6 + 6(R + s)\sin\{q(R + s)\}/q^5 + \{q^4Rs^3 - 6q^2s(R - s) - 24\}\cos(qR)/q^6 + \{q^2s^2(3R - s) - 6(R - 3s)\}\sin(qR)/q^5] \tag{33}$$

where

$$C_{\text{norm},2}{}^{-1} = s^4(15R^2 + 6Rs + s^2)/15 \tag{34}$$

The corona scattering can then be written as

$$A_{\text{chain}}(q) = \frac{[A_1(q) + a_1A_2(q)]}{(1 + a_1)}\exp(-q^2\sigma^2/2) \tag{35}$$

For the *Spline3* the radial density is given by a linear combination of (28), (29), and

$$\rho_3(r) = [4(R - r)^3 - (R - r - s)^3]/(4s^3) \quad \text{for } R \le r < R + s$$

$$\rho_3(r) = [4(r - R - 2s)^3 - (r - R - 3s)^3]/(4s^3) \quad \text{for } R + s \le r < R + 2s$$

$$\rho_3(r) = -(r - R - 3s)^3/(4s^3) \quad \text{for } R + 2s \le r < R + 3s$$

$$\rho_3(r) = 0 \quad \text{elsewhere} \tag{36}$$

The total profile is thus

$$\rho_{\text{chain}}(r) = [\rho_1(r) + a_1\rho_2(r) + a_2\rho_3(r)]/(1 + a_1 + a_2) \tag{37}$$

where a_1 and a_2 are fitting parameters. The Fourier transform of $\rho_3(r)$ is

$$A_3(q) = C_{\text{norm},3}[24\cos\{q(R + 3s)\}/q^6 + 6(R + 3s)\sin\{q(R + 3s)\}/q^5 - 96\cos\{q(R + 2s)\}/q^6 - 24(R + 2s)\sin\{q(R + 2s)\}/q^5 + 144\cos\{q(r + s)\}/q^6 + 36(r + s)\sin\{q(r + s)\}/q^5 + [q^4rs^3 - 6q^2s(r + s) - 72]\cos(qr)/q^6 - \{q^2s^2(3r + s) + 18(r - s)\}\sin(qr)/q^5] \tag{38}$$

where

$$C_{\text{norm},3}{}^{-1} = s^4(345r^2 + 726rs + 479s^2)/60 \tag{39}$$

The corona scattering can then be written as

$$A_{\text{chain}}(q) = \frac{[A_1(q) + a_1A_2(q) + a_2A_3(q)]}{(1 + a_1 + a_2)}\exp(-q^2\sigma^2/2) \tag{40}$$

The scaling theory of Halperin[9] suggests for a swollen corona of a micelle a power-law profile with an $r^{-4/3}$ behavior. For this *PowFix* profile we used

$$\rho_{\text{chain}}(r) = Cr^{-4/3}\exp[-(r/r_o)^\beta] \tag{41}$$

where C is a normalization constant and $\exp[-(r/r_o)^\beta]$ is a cutoff function which has to be used due to the finite length of the corona chains. r_o and β are fitting parameters. In the fits, the profile was Fourier transformed numerically.

The last form we applied for the profile was a power-law profile with an arbitrary exponent, which is a generalization of the previous scaling profile. This *PowFit* profile was described by

$$\rho_{\text{chain}}(r) = Cr^{-\alpha}\exp[-(r/r_o)^\beta] \tag{42}$$

where α is also a fitting parameter. Also this expression was Fourier transformed numerically. For this profile and the PowFix profile, it was checked that the results were independent of the integration method used for the Fourier transformation.

References and Notes

(1) Hamley, I. W. *The Physics of Block Copolymers*; Oxford University Press: Oxford, England, 1998.
(2) See, e.g., Dan, N.; Tirrell, M. *Macromolecules* **1992**, *25*, 2890. Wijmans, C. M.; Zhulina, E. B. *Macromolecules* **1993**, *26*, 7214. McConnell, G. A.; Gast, A. P. *Phys. Rev. E* **1996**, *54*, 5447. Lin, E. K.; Gast, A. P. *Macromolecules* **1996**, *29*, 390.

(3) McConnell, G. A.; Lin, E. K.; Gast, A. P.; Huang, J. S.; Lin, M. Y.; Smith, S. D. *Faraday Discuss.* **1994**, *98*, 121.
(4) See, e.g., Murat, M.; Grest, G. S. *Macromolecules* **1991**, *24*, 704. Lai, P. Y.; Binder, K. *J. Chem. Phys.*, **1991**, *95*, 9288. Toral, R.; Chakrabarti, A. *Phys. Rev. E* **1993**, *47*, 4240. Neelov, I. M.; Binder, K. *Macromol. Theory Simul.* **1995**, *4*, 119.
(5) Svaneborg, C.; Pedersen, J. S. *J. Chem. Phys.* **2000**, *112*, 9661.
(6) Svaneborg, C.; Pedersen, J. S. *Phys. Rev. E* **2001**, *64*, 010802-(R).
(7) Svaneborg, C.; Pedersen, J. S. *Macromolecules* **2002**, *35*, 1028.
(8) Alexander, S. *J. Phys. (Paris)* **1977**, *38*, 983. de Gennes, P. G. *Macromolecules* **1980**, *13*, 1069.
(9) Halperin, A. *Macromolecules* **1987**, *20*, 2943.
(10) See, e.g., Pedersen, J. S. *Adv. Colloid Interface Sci.* **1997**, *70*, 171, and Pedersen, J. S.; Svaneborg, C. *Curr. Opin. Colloid Interface Sci.* **2002**, *7*, 158.
(11) Iatrou, H.; Willner, L.; Hadjichristidis, N.; Halperin, A.; Richter, D. *Macromolecules* **1996**, *29*, 582.
(12) Richter, D.; Schneiders, D.; Monkenbusch, M.; Willner, L.; Fetters, L. J.; Huang, J. S.; Lin, M.; Mortensen, K.; Farago, B. *Macromolecules* **1997**, *30*, 1053.
(13) Ramzi, A.; Prager, M.; Richter, D.; Efstratiadis, V.; Hadjichristidis, N.; Young, R. N.; Allgaier, J. B. *Macromolecules* **1997**, *30*, 7171.
(14) Poppe, A.; Willner, L.; Allgaier, J.; Stellbrink, J.; Richter, D. *Macromolecules* **1997**, *30*, 7462.
(15) Nakano, M.; Matsuoka, H.; Yamaoka, H.; Poppe, A.; Richter, D. *Macromolecules* **1999**, *32*, 697.
(16) Goldmint, I.; Yu, G.-E.; Booth, C.; Smith, K. A.; Hatton, T. A. *Langmuir* **1999**, *15*, 1651.
(17) Pedersen, J. S.; Hamley, I. W.; Ryu, C. Y.; Lodge, T. P. *Macromolecules* **2000**, *33*, 542.
(18) Mortensen, K.; Pedersen, J. S. *Macromolecules* **1993**, *26*, 805.
(19) Chu, B.; Wu, G.; Schneider, D. K. *J. Polym. Sci., Part B* **1994**, *32*, 2605.
(20) Liu, Y.; Chen, S.-H.; Huang, J. S. *Macromolecules* **1998**, *31*, 2236.
(21) Goldmint, I.; von Gottberg, F. K.; Smith, K. A.; Hatton, T. A. *Langmuir* **1997**, *13*, 3659.
(22) King, S. M.; Heenan, R. K.; Cloke, V. M.; Washington, C. *Macromolecules* **1997**, *30*, 6215.
(23) Appell, J.; Porte, G.; Rawiso, M. *Langmuir* **1998**, *14*, 4409.
(24) Förster, S.; Burger, C. *Macromolecules* **1998**, *31*, 879.
(25) Pedersen, J. S.; Gerstenberg, M. C. *Macromolecules* **1996**, *29*, 1363.
(26) Pedersen, J. S. *J. Appl. Crystallogr.* **2000**, *33*, 637.
(27) Pedersen, J. S. *J. Chem. Phys.* **2001**, *114*, 2839.
(28) Derici, L.; Ledger, S.; Mai, S.-M.; Booth, C.; Hamley, I. W.; Pedersen, J. S. *Phys. Chem. Chem. Phys.* **1999**, *1*, 2773.
(29) Leclerc, E.; Calmettes, P. *Physica B* **1997**, *241* 1141.
(30) Plestil, J.; Kriz, J.; Tuzar, Z.; Prochazka, K.; Melnichenko, Y. B.; Wignall, G. D.; Talingting, M. R.; Munk, P.; Webber, S. E. *Macromol. Chem. Phys.*, **2001**, *202*, 553. Plestil, J.; Pospisil, H.; Kadlec, P.; Tuzar, Z.; Kriz, J.; Gordeliy, V. I. *Polymer* **2001**, *42*, 2941.
(31) Borbely, S. *Langmuir* **2000**, *16*, 5540. Borbely, S.; Pedersen, J. S. *Physica B* **2000**, *276*, 363.
(32) Pedersen, J. S.; Laso, M.; Schurtenberger, P. *Phys. Rev. E* **1996**, *54*, R5917.
(33) Pedersen, J. S.; Schurtenberger, P. *Macromolecules* **1996**, *29*, 7602.
(34) Pedersen, J. S.; Schurtenberger, P. Unpublished work. Pedersen, J. S.; Schurtenberger, P. *Europhysics Lett.* **1999**, *45*, 666.
(35) Förster, S.; Wenz, E.; Lindner, P. *Phys. Rev. Lett.* **1996**, *77*, 95.
(36) Won, Y. Y.; Davis, H. T.; Bates, F. S.; Agamalian, M.; Wignall, G. D. *J. Phys. Chem. B* **2000**, *104*, 7134. *J. Phys. Chem. B* **2000**, *104*, 9054.
(37) Willner, L.; Poppe, A.; Allgaier, J.; Monkenbusch, M.; Lindner, P.; Richter, D. *Europhys. Lett.* **2000**, *51*, 628.
(38) Morton, M.; Fetters, L. J. *Rubber Chem. Technol.* **1975**, *48* 359.
(39) Pedersen, J. S. in: *Modern Aspects of Small-angle Scattering.* Brumberger, H., Ed.; Kluwer Academic Press: Dordrecht, The Netherlands, 1995; p 57.
(40) Price, C.; McAdam, J. D. G.; Lally, T. P.; Woods, D. *Polymer* **1974**, *15*, 228.
(41) Bahadur, P.; Sastry, N. V.; Marti, S.; Riess, G. *Colloids Surf.* **1985**, *16*, 337.
(42) Higgins, J. S.; Blake, S.; Tomlins, P. E.; Ross-Murphy, S. B.; Staples, E.; Penfold, J.; Dawkins, J. V. *Polymer* **1988**, *29*, 1968.
(43) McConnell, G. A.; Lin, M. Y.; Gast, A. P. *Macromolecules* **1995**, *28* 1995, 6754.
(44) Press, W. H.; Flannery, B. P.; Teukolsky, S. A.; Vetterling, W. T. *Numerical Recipies.* Cambridge University Press: Cambridge, England, 1989.
(45) Yan, Y. D.; Clarke J. H. R. *J. Chem. Phys.* **1990**, *93*, 4501.
(46) Pedersen, J. S. *Curr. Opin. Colloid Interface Sci.*, **1999**, *4*, 190.
(47) Ashcroft, N. W.; Lekner, J. *Phys. Rev.* **1966**, *83*, 145.
(48) Kinning, D. J.; Thomas, E. L. *Macromolecules* **1984**, *17*, 1712.
(49) Vrij, A. *J. Chem. Phys.* **1979**, *71*, 3267.
(50) Mortensen, K. *Curr. Opin. Colloid Interface Sci.* **1998**, *3*, 12 and references therein.
(51) Jain, N. J.; Aswal, V. K.; Goyal, P. S.; Bahadur, P. *J. Phys. Chem. B* **1998**, *102*, 8452; *Colloids Surf. A* **2000**, *173*, 85.
(52) Alexandridis, P.; Yang, L. *Macromolecules* **2000**, *33*, 3382; *Macromolecules* **2000**, *33*, 5574. Yang, L.; Alexandridis, P.; Steytler, D. C.; Kositza, M. J.; Holzwarth, J. F. *Langmuir* **2000**, *16*, 4819. Yang, L.; Alexandridis, P. *Langmuir* **2000**, *16*, 8555.
(53) Perreur, C.; Habas, J. P.; Peyrelasse, J.; Francois, J.; Lapp, A. *Phys. Rev. E* **2001**, 031505.
(54) Pedersen, J. S.; Posselt, D.; Mortensen, K. *J. Appl. Crystallogr.* **1990**, *23*, 321.
(55) Bevington, B. R. *Data reduction and error analysis for the physical sciences*; McGraw-Hill: New York, 1969.
(56) Fetters, L. J.; Hadjichristidis, N.; Lindner, J. S.; Mayes, J. W. *J. Phys. Chem. Ref. Data* **1994**, *23*, 619.
(57) Aharoni, S. M. *Macromolecules* **1983**, *16*, 1722.
(58) Note that the two weighting terms $w(qR_g)$ and $[1 - w(qR_g)]$ should be interchanged in the expression in ref 33.

MA0204913